

JGR Atmospheres

RESEARCH ARTICLE

10.1029/2021JD035556

Key Points:

- The relative roles of terrain, surface roughness, and cold pool outflows in the formation of heavy rainfall were investigated
- A convergence line associated with winds affected by underlying surface, cold pool outflows, and persistent southerly flows was favorable
- Land-sea surface roughness contrast and terrain played an important role in the initial formation of the convergence line

Supporting Information:

Supporting Information may be found in the online version of this article.

Correspondence to:

H. Li and Y. Huang,
lihq529@163.com;
huangynj@gmail.com

Citation:

Li, H., Huang, Y., Hu, S., Wu, N., Liu, X., & Xiao, H. (2021). Roles of terrain, surface roughness, and cold pool outflows in an extreme rainfall event over the coastal region of South China. *Journal of Geophysical Research: Atmospheres*, 126, e2021JD035556. <https://doi.org/10.1029/2021JD035556>

Received 12 JUL 2021
Accepted 15 NOV 2021

Roles of Terrain, Surface Roughness, and Cold Pool Outflows in an Extreme Rainfall Event Over the Coastal Region of South China

Huiqi Li^{1,2} , Yongjie Huang³ , Sheng Hu¹, Naigeng Wu⁴, Xiantong Liu¹, and Hui Xiao¹

¹Institute of Tropical and Marine Meteorology, China Meteorological Administration, Guangzhou, China, ²State Key Laboratory of Severe Weather, Chinese Academy of Meteorological Sciences, Beijing, China, ³Center for Analysis and Prediction of Storms, University of Oklahoma, Norman, OK, USA, ⁴Guangdong Ecological Meteorology Center, Guangzhou, China

Abstract An extreme rainfall event with maximum 12 hr accumulated rainfall of 464.8 mm associated with a quasi-stationary mesoscale convective system occurred over the western coastal region of South China in June 2017. An observational analysis shows that early convective storms were initiated near the mountains and moved northeastwards. Moreover, a convergence line between cold northerly winds and warm southerly winds in the lower levels was formed, which favored the development of the quasi-stationary system. Cold northerly winds were associated with land breeze, downslope winds as well as previous rainfall during earlier period, and cold pool outflows during later period. Cloud-resolving simulations were performed to examine the roles of terrain, land-sea surface roughness contrast, and cold pool outflows in the formation of heavy rainfall. Results demonstrate that land-sea surface roughness contrast and mountains in the middle of Yangjiang and Jiangmen facilitated the formation of the convergence line during earlier period, and cold pool outflows sustained it during later period. Besides orographic lifting, coastal hills helped reduce the stability. Mountains in the middle of Yangjiang hindered the movement of the convective system, without which the associated heavy rainfall would shift farther north. Mt. Tianlu with westward concave morphology played a vital role in the formation of local convergence and the concentration of heavy rainfall. Without it, the total rainfall in the region of interest was reduced. This study suggests the importance of representing processes associated with the complex underlying surface in models for the prediction of heavy rainfall in coastal regions.

1. Introduction

Many coastal regions in the world are hotspots for heavy rainfall, for example, the South China (Luo et al., 2017), India (Romatschke & Houze, 2011), the eastern United States (Hitchens et al., 2013; Lombardo & Colle, 2010), Brazil (Mattos & Machado, 2011; Rodrigues & Ynoue, 2016), and Mediterranean (Cohuet et al., 2011; Duffourg et al., 2015). Complex underlying surface and associated horizontal heterogeneities in low-level temperature, moisture, and winds over the coastal regions greatly challenge the forecasts for heavy rainfall. The behavior of storms varies in different coastal environments with different topographical settings. Under a weakly forced synoptic environment, mesoscale boundaries which indicate lifting are crucial for the heavy rainfall over the coastal regions. The mesoscale boundaries can originate from land surface heterogeneities (e.g., land-sea contrast), differential latent heating/cooling (e.g., cool pool outflows), etc. The mesoscale boundaries are usually evident as mesoscale boundary-layer convergence lines along which horizontal convergence of the airflow occurs. The location and intensity of rainfall are affected by the factors that influence the convergence lines, for example, local terrain, land-sea contrast, and cold pool outflows.

Orographic effects on the development of convection have been well documented. Lifting of moist flow by a mountain can trigger deep convection (Caracena et al., 1979; Marwitz, 1983; Rasmussen & Houze, 2016; Weckwerth et al., 2014). Convergence between downslope flows and low-level moist flows also favors the development of deep convection (Houze, 2012; C. C. Wang et al., 2005). Moreover, terrain morphology is noticed to regulate wind direction and speed (Whiteman, 2000), thus affecting the location of convergence and convection. Such cases have been found in the Alps (Schneidereit & Schär, 2000), Taiwan (Lin et al., 2001), Himalayan (Houze et al., 2007; Romatschke et al., 2010), Beijing (H. Li et al., 2017a, 2017b), etc. Although the orographic effects have been widely studied, the detailed mechanisms may be quite different in different climate zones, or even in different locations of a climate zone, and necessitate more specific study. How the representation of terrain

features especially their small-scale features affects the quantitative simulation of heavy rainfall over the mountainous region is another issue worth further investigation.

In coastal regions, horizontal temperature gradient due to different heating capacity between soil and water generates land/sea breeze circulations. Convergence or mesoscale disturbance associated with land/sea breezes provides favorable conditions for convective initiation (CI; Byers & Rodebush, 1948). Many case studies about heavy rainfall over different regions demonstrate that land/sea breeze circulations have significant impacts on the development of convection, for example, in Florida (Baker et al., 2001; Kingsmill, 1995), Guangdong (Liu et al., 2001; Meng et al., 2014), Darwin (Wapler & Lane, 2012), Taiwan (Miao & Yang, 2020; Tu et al., 2014), Hainan Island (Liang et al., 2017). However, strong synoptic winds may obscure land/sea breezes (Arritt, 1993). In addition, interaction between land/sea breezes and orographic effects modulates the formation of convergence and moisture distribution, making the location of CI more variable (Barthlott & Kirshbaum, 2013; Liang et al., 2017; Tu et al., 2014; C. C. Wang & Kirshbaum, 2015). Compared with difference in temperature, discontinuity in surface roughness between land and sea is less discussed to date. Lean et al. (2009) found that roughness effect was the primary cause for the initial formation of the convergence line which was the key factor in the development of a thunderstorm in southern England. Lee et al. (2019) concluded from a case study of coastal precipitation over Korean Peninsula that roughness discontinuity made great contribution to the formation of convergence zone.

It has been well known that cold outflow boundaries resulting from pre-existing precipitation systems can trigger convection (e.g., Huang, Liu, Liu, & Knievel, 2019; Huang, Liu, Liu, Li, & Knievel, 2019; Khairoutdinov & Randall, 2006; Lima & Wilson, 2008; Purdom, 1976; Weckwerth & Wakimoto, 1992; Wilhelmson & Chen, 1982; Wilson & Mueller, 1993). The interaction of cold pool with environmental conditions affects the evolution of convection (e.g., James et al., 2005; Rotunno et al., 1988; Weisman & Rotunno, 2004). The roles of cold pool depend on the convective lifecycle stage, and vary under different surface conditions (e.g., Dai et al., 2021). Dai et al. (2021) and Grant et al. (2018) found that even with weakened cold pools, the convection can be enhanced in their simulations because of more upright updrafts between the cold pool and the environment in later stages, or due to less entrainment of cold pool air into updrafts. In the presence of topography, the impact of cold pool outflows on the development of convection involves more complex processes. Bennett et al. (2011) and Corsmeier et al. (2011) showed that cold-pool outflows or gust front from previous precipitation systems interacting with thermal flows over complex terrain enhanced convergence and the development of convection near the Black Forest Mountains. Xu et al. (2012) revealed that high terrain in Taiwan trapped the cold pool and sustained the long-lived mesoscale convective system over the upstream ocean and southwest coast of Taiwan. When it comes to the mountainous coastal regions, the processes become even more complicated under the influence of ocean, for example, marine atmospheric boundary layer (MABL) and land/sea breeze. F. Wu and Lombardo (2021) conducted idealized numerical simulations to reveal that the collision between the descending storm outflows and a moving MABL could lead to intense storm and precipitation over the sloping terrain.

The western coastal region of South China is characterized by the inland Mts. Yunwu and Tianlu, some hills near the coastlines (e.g., Mt. Longgao), and South China Sea on the south (Figure 1a). Heavy rain frequently hits the western coast of South China during the pre-summer rainy season (April–June) posing a threat to lives and property safety (N. Wu et al., 2020; Zhong & Tian, 2020). Statistical studies reveal that CI and extremely heavy rainfall occur even more frequently over the western coast than the eastern coast of South China (Bai et al., 2020; N. Wu et al., 2020). Most extreme hourly rainfall (more than 40%) over the coastal region of South China during the pre-summer rainy season occurs under weak synoptic forcing (Luo et al., 2016), and quantitative precipitation forecast (QPF) skill for the extreme rainfall remains poor. A better understanding of how different factors (e.g., terrain, land-sea contrast, and cold pools) combine to influence the heavy rainfall under weak synoptic forcing over the western coast is essential for improving QPF skill. However, unlike the central and eastern coast of South China (e.g., Du, Chen, Han, Bai, & Li, 2020; Du, Chen, Han, Mai, et al., 2020; Huang, Liu, Liu, & Knievel, 2019; Huang, Liu, Liu, Li, & Knievel, 2019), few studies have elucidated the relative roles of these factors in the formation of heavy rainfall over the western coast. Previous study (e.g., H. Wang et al., 2014) revealed the lifting mechanism by mesoscale boundaries over the western coast through observational analysis but the relative contribution of different factors remained to be further explored due to the limitation in observations. Therefore, in the present study, an extremely heavy rainfall event over the western coast of South China occurring during June 21–22, 2017 is selected to investigate the roles of different factors in the formation of heavy rainfall through

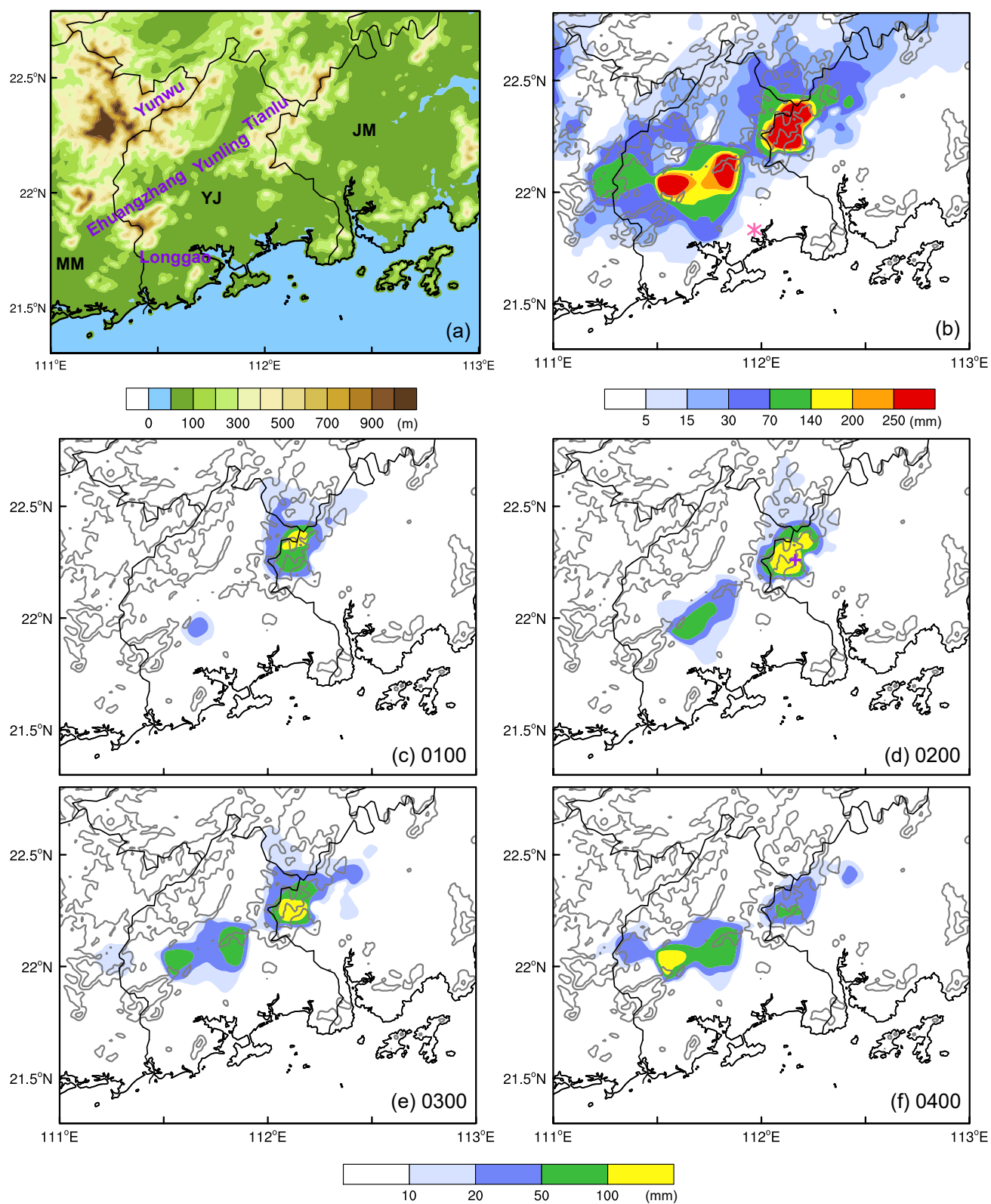


Figure 1.

analyses of observations and numerical simulations. This event is selected for a few reasons. It breaks the records of 1 and 3 h accumulated rainfall for Jiangmen with 165 and 365.1 mm respectively. Moreover, the heavy rainfall was localized and concentrated near mountains about 50 km away from the coastlines, which provides a good example to study the combined effects of terrain and land-sea contrast. The operational numerical models failed to predict this extreme rainfall. Two main questions as follows will be addressed in this study:

- What are the relative roles of mountains in different locations, land-sea contrast in surface roughness, and cold pool outflows in the initiation and maintenance of convective storms?
- To what extent do these factors affect the intensity and location of rainfall?

The next section provides an overview and observational analysis of the selected case. Section 3 describes the model configuration as well as the design of sensitivity experiments, and the verification of the control simulation (CNTL). Section 4 discusses the roles of different factors through comparison between sensitivity experiments and the CNTL. A summary and conclusions are given in the final section.

2. Observational Analysis

From the night of June 21 to the morning of June 22, 2017, heavy rainfall occurred in the western coastal region of South China, mainly in Yangjiang and Jiangmen, with maximum 12 h accumulated rainfall from 20:00 LST (=UTC + 8 h) June 21 to 08:00 LST June 22 reaching 464.8 mm. The 12 h accumulated rainfall exhibited a southwest-northeast oriented band closely related to the mountains (Figure 1b). The extreme rainfall (12 h accumulated rainfall ≥ 250 mm) mainly concentrated in the east of Mt. Tianlu and in the area with relatively low altitudes between Mts. Yunwu and Tianlu. Intense hourly rainfall more than 100 mm was first observed near Mt. Tianlu from 01:00 to 04:00 LST June 22 (Figures 1c–1e), and then in the middle of Yangjiang from 04:00 LST June 22 (Figure 1f). Extreme hourly rainfall of 165 mm was observed in Datian, Jiangmen (denoted by a plus mark in Figure 1d) from 02:00 to 03:00 LST June 22.

2.1. Synoptic Situation

Figures 2a and 2b show that a weak trough at 500 hPa approached Guangdong province from the west. Meanwhile, the subtropical high was extending westwards, and the 5,880 gpm isobar already reached the coastline of Guangdong province at 20:00 LST June 21 (Figure 2a). Guangdong province was located between the weak trough and the subtropical high, which was conducive to the development of convection (Figure 2b). At the middle and lower troposphere, southwesterly wind prevailed over Guangdong. Sea surface temperature near Yangjiang and Jiangmen remained $\sim 29^{\circ}\text{C}$ during this rainfall event, about 1°C higher than that near the eastern coast of Guangdong (not shown). Southwesterly winds continuously transported warm and moist air into the region of heavy rainfall. As the subtropical high extended westwards, southwesterly wind over the sea adjacent to Guangdong gradually turned to be southerly (Figure 2b). The wind speed at 850 hPa over Guangxi, Guangdong, and the adjacent sea got stronger ($> 12 \text{ m s}^{-1}$), forming a southerly low-level jet. Cross-sections of horizontal wind speed along 111.75°E show that the low-level jet appeared farther south over the sea at 20:00 LST June 21 but at a lower level of ~ 950 hPa (Figure 2c). Then the low-level jet extended higher and northwards to the land with a high-speed core of $\sim 13 \text{ m s}^{-1}$ at ~ 900 hPa at 02:00 LST June 22 (Figure 2d). This pattern of the jet was similar to the statistical result in Z. Li et al. (2020). The lower-level jet at ~ 950 hPa resulted in convergence near the coastline while the jet at a higher level (~ 900 hPa) led to divergence above. As a result, convergence in the boundary layer coupled with divergence aloft was present near the coast, which was beneficial to the development of upward motion and the occurrence of convection. Furthermore, the low-level jet facilitated the transport of moisture.

A morning sounding at Yangjiang (blue profiles in Figure 3) indicates a moist layer from the surface up to about 450 hPa. It remained moist below 500 hPa in the sounding at 20:00 LST June 21 (red profiles in Figure 3) while it

Figure 1. (a) Terrain over Yangjiang and Jiangmen (shaded, m). The cities' names are abbreviated as follows: JM (Jiangmen), MM (Maoming), YJ (Yangjiang). The mountains mentioned in the text are labeled in purple. (b) 12 hr accumulated rainfall from 20:00 LST June 21 to 08:00 LST June 22, 2017 based on rain gauge observations (shaded, mm). The location of Yangjiang station is denoted by a pink star. (c–f) Hourly rainfall starting from (c) 01:00, (d) 02:00, (e) 03:00, (f) 04:00 LST June 22, 2017, respectively. The purple plus mark in (d) denotes the location of maximum hourly rainfall. Terrain heights are contoured by gray lines at 200 and 500 m; similarly for the rest of the figures.

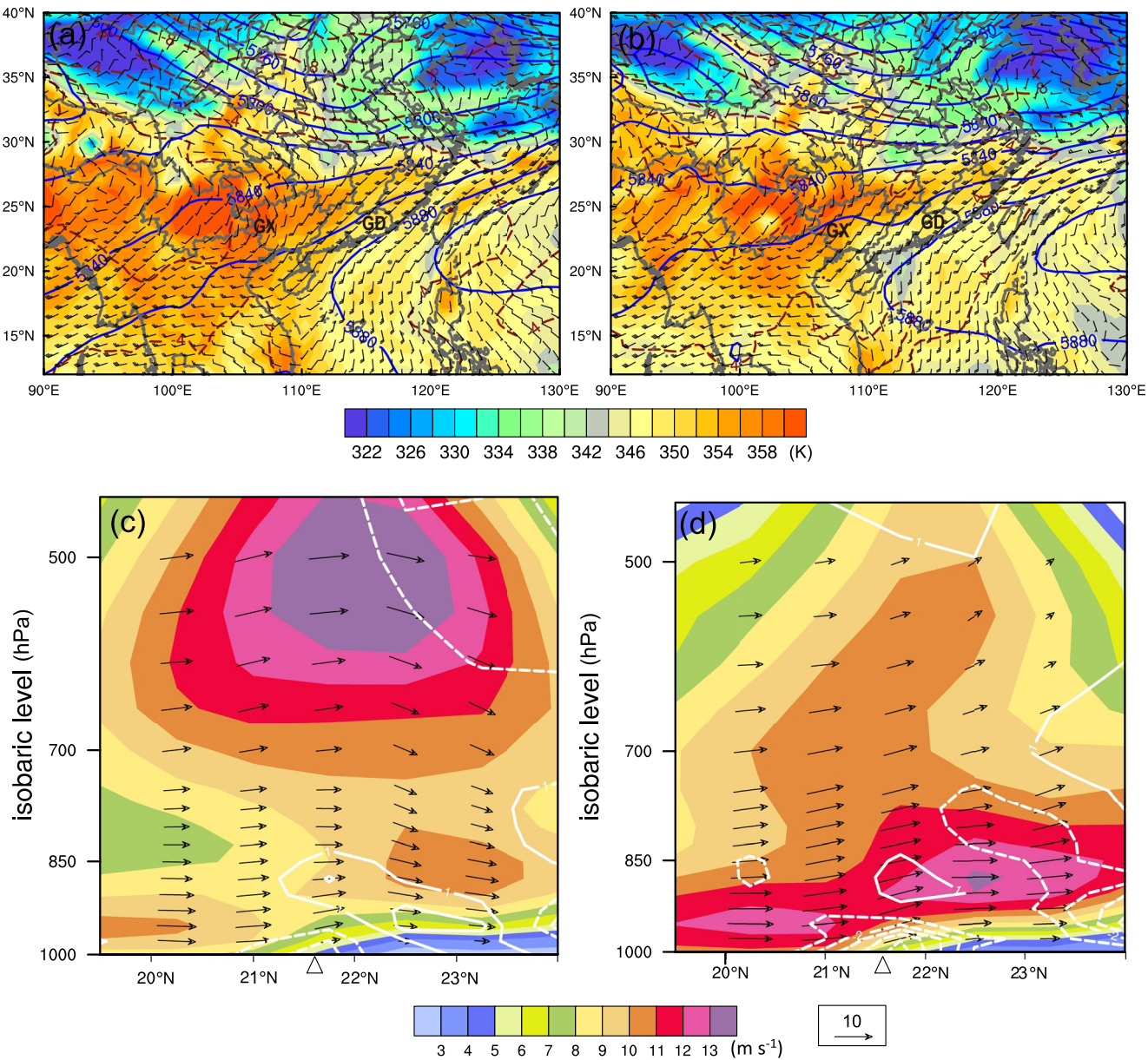


Figure 2. The ERA-Interim reanalysis at 20:00 LST June 21 (left column), and 02:00 LST June 22, 2017 (right column). (a, b) Geopotential height (solid blue contours at intervals of 20 gpm) and temperature (dashed red contours at intervals of 2°C) at 500 hPa, winds (a full barb is 4 m s⁻¹) and equivalent potential temperature (shaded, K) at 850 hPa. Guangdong and Guangxi provinces are marked as GD and GX respectively in the figures. (c, d) Vertical cross-sections along 111.75°E of horizontal wind speed (shaded, m s⁻¹), divergence (dashed white contours for $-5, -4, \dots, -1 \times 10^{-5}$ s⁻¹, solid white contours starting at 1×10^{-5} s⁻¹ at intervals of 1×10^{-5} s⁻¹), and in-plane wind vectors with vertical motion (w) amplified by a factor of 100. The triangle indicates the position of coastline.

became moister above 350 hPa compared with that at 08:00 LST. A dry layer existed in the middle layer from 500 to 350 hPa in the sounding at 20:00 LST. It is notable that temperature below 150 hPa at 20:00 LST was generally higher than that at 08:00 LST. Both soundings show gradual veering of southwesterly winds at lower levels to northwesterly winds at 300 hPa, and then northeasterly winds at 250 hPa, indicating the presence of weak warm advection through the mid-lower troposphere. At 20:00 LST, very small convective inhibition (CIN, 0.7 J kg⁻¹), low lifting condensation level (LCL, ~980 hPa) and level of free convection (LFC, ~972 hPa) imply that only small lifting was needed to initiate convection. Rather large surface-based CAPE (~3,480 J kg⁻¹) suggests that unstable and moist conditions were favorable for the development of convection.

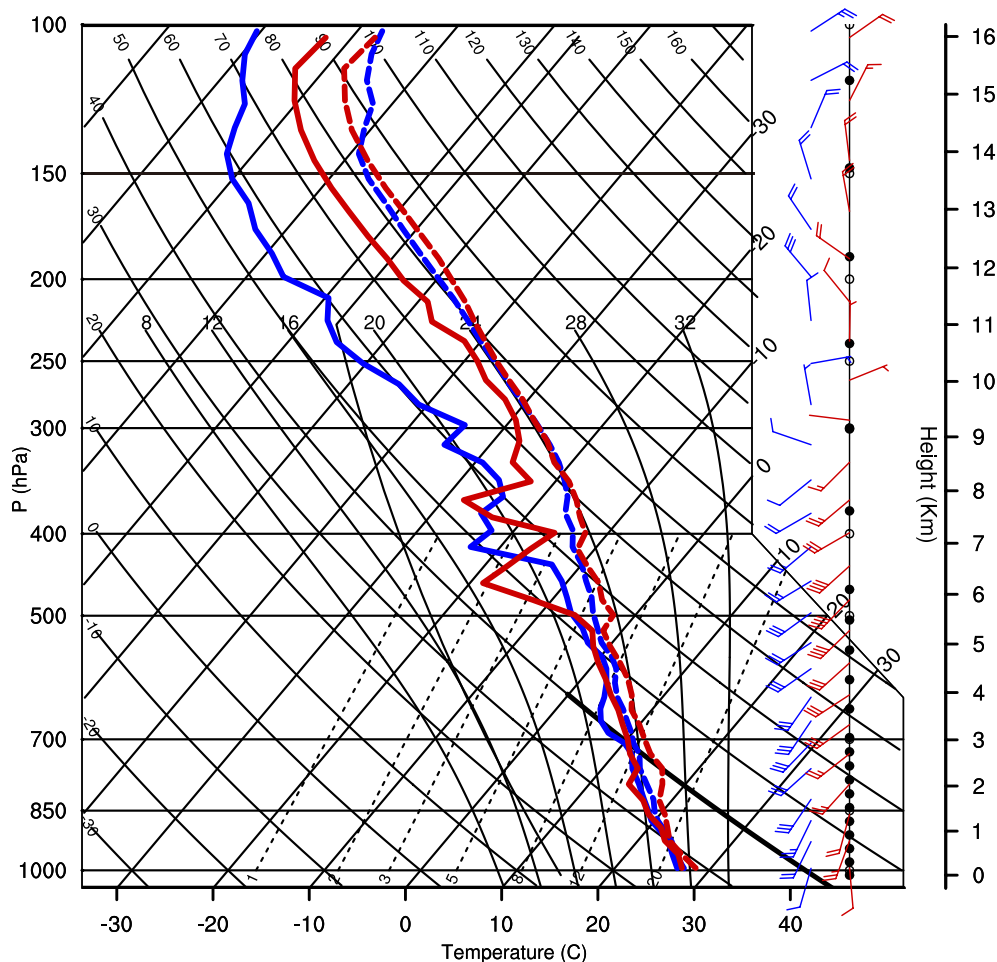


Figure 3. Soundings were taken at Yangjiang station (see Figure 1b for its location) at 08:00 (blue) and 20:00 (red) LST June 21, 2017.

2.2. Radar Observations

Composite radar reflectivity in Figure 4 shows the evolution of the precipitation system. Precipitation mainly occurred in the inland mountainous area in the afternoon of June 21. Around 22:30 LST, new convective storms initiated on the south (windward) side of Mt. Tianlu, and then intensified when moving northeastwards. Meanwhile, new convective storms also developed on the north of Mt. Longgao near the coastline, and moved northeastwards (Figures 4a–4c). These convective storms experienced upscale growth and organized into a southwest-northeast oriented convective band after 01:30 LST June 22 with intense convective core in the east of Mt. Tianlu and the area with low altitudes between Mts. Yunwu and Tianlu (Figure 4d). This quasi-stationary convective band maintained for about 4 h, resulting in the extremely heavy rainfall. Around 05:00 LST June 22, three short southwest-northeast oriented convective bands were formed in the middle of Yangjiang (Figure 4g), and continued to bring heavy rainfall there (Figure 1f). Afterward, the convection gradually weakened, and moved northwards.

Radial velocity at the elevation angle of 0.5° from Yangjiang radar in Figure 5 shows that southerly winds predominated over the observed region. Radial winds approaching toward the radar was found near Mts. Ehuangzhang and Yunwu, indicating the existence of northerly or northwesterly flows probably related to downslope winds (Figure 5a). Convergence was formed between these northerly-northwesterly flows and ambient southerly flows. After 01:12 LST June 22, radial winds toward the radar appeared near the opening (i.e., east) of the westward concave region of Mt. Tianlu (Figure 5c), which were associated with cold pool outflows. It also suggests the enhancement of convergence zone near this area. After 03:24 LST June 22, the radial winds toward the radar over this region gradually disappeared as the intense convection weakened and moved away from this region.

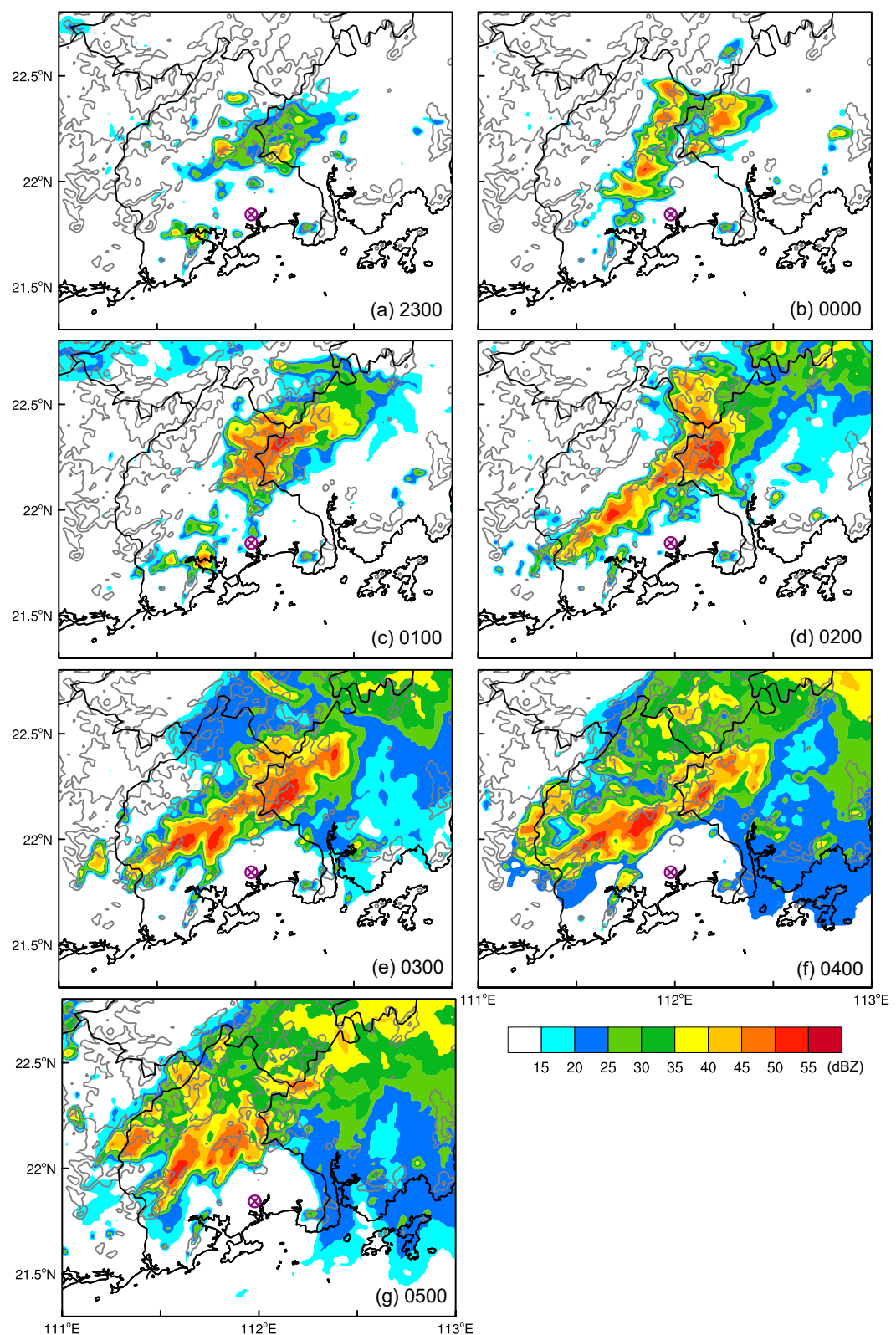


Figure 4. Composite radar reflectivity (dBZ) observed by Yangjiang's radar (marked by the crossed circles in the figures) at (a) 23:00 LST June 21, (b) 00:00, (c) 01:00, (d) 02:00, (e) 03:00, (f) 04:00, and (g) 05:00 LST June 22, 2017.

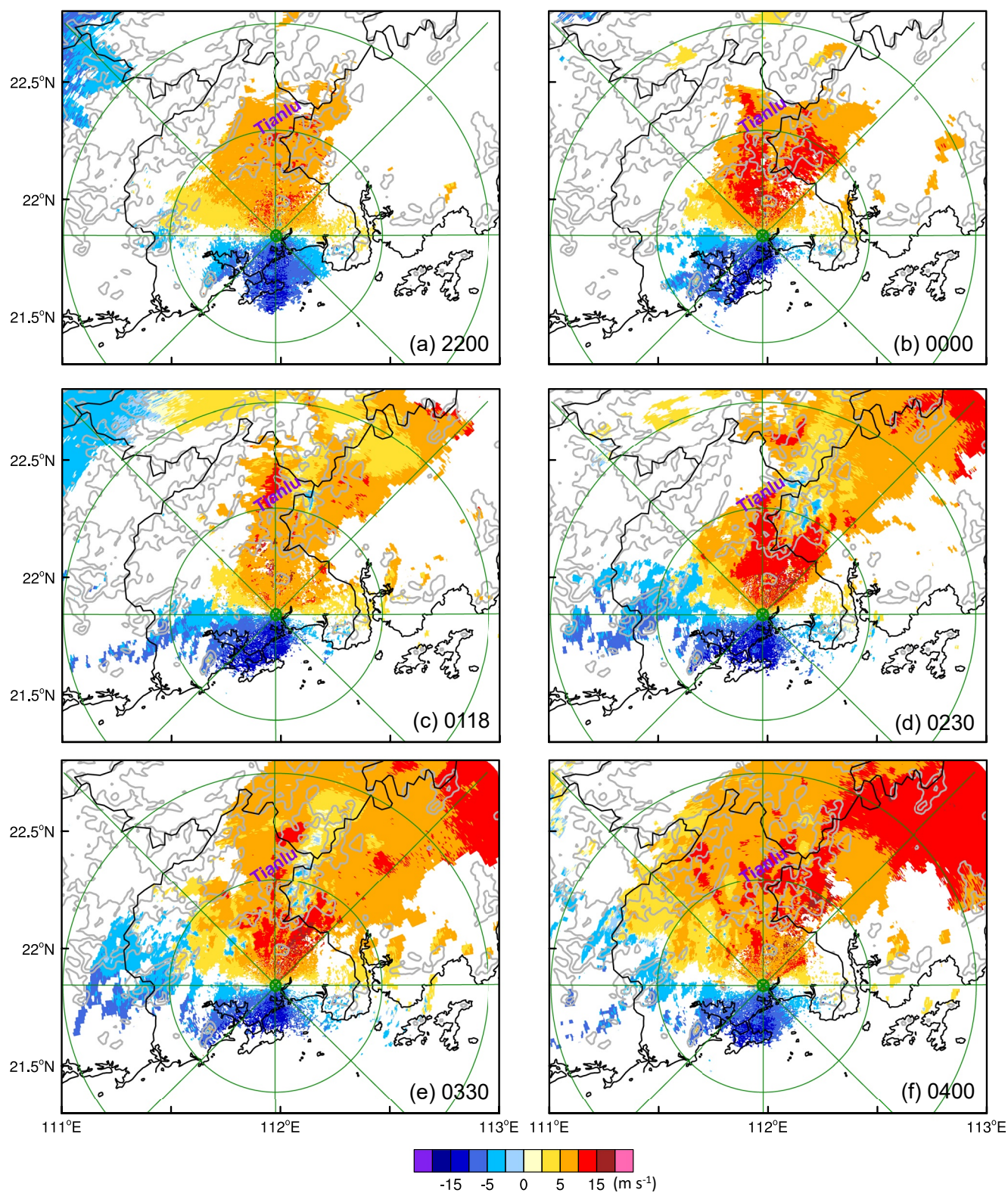


Figure 5. Radial velocity (shaded, m s^{-1}) at the elevation angle of 0.5° at (a) 22:00 LST June 21, (b) 00:00, (c) 01:18, (d) 02:30, (e) 03:30, (f) 04:00 LST June 22, 2017. The green circles denote the ranges of 50, and 100 km from the Yangjiang's radar (represented by the crossed circles).

(Figures 5e and 5f). This period with radial winds toward the radar near Mt. Tianlu coincided with the maximum hourly rainfall (i.e., 02:00–03:00 LST June 22) during this event.

2.3. Surface Observations

Surface observations at 22:00 LST June 21 present that cold northerly winds (some land breezes and downslope winds) prevailed in the northern mountainous area while warm southerly winds remained in the southern coastal area (Figure 6a). The cold air in the mountainous area was not only caused by cooling at night but also affected by previous rainfall. Northerly winds were weak, which was probably associated with complex terrain and large surface roughness in the northern area. In contrast, land breezes did not develop near the coast, and winds over there were predominantly driven by large-scale flow. Southerly winds near the coast continually transported warm moist air from the ocean. A southwest-northeast oriented convergence line as well as thermal boundary between the cold northerly winds and warm southerly winds can be clearly seen in the middle of Yangjiang (indicated by dashed pink lines in Figure 6). This mesoscale boundary favored the development, organization, and maintenance of convection. In addition, the westerly and southerly winds impinged on and were lifted by Mt. Tianlu, which also facilitated CI. After 00:00 LST June 22, the convergence line somewhat weakened as southerly winds grew stronger and intruded further inland. As the convective band formed and maintained in the middle of Yangjiang and Jiangmen, the convectively induced outflows enhanced the northerly flows (Figure 6e). The speed of the northerly flows became more comparable to the speed of the southerly flows on the south side of the convergence line. Consequently, the convergence between them was enhanced again, which was evident in the east of Mt. Tianlu. This convergence line between northerly outflows and southerly flows continued to support the maintenance of the convective system. After 04:00 LST June 22, the southerly winds in Jiangmen retreated to farther south and became weaker, and instead cold northerly winds were dominant (Figure 6f), leading to the weakening of convection due to insufficient energy supply from the southerly winds. On the other hand, southerly winds in Yangjiang did not weaken markedly, and thus the convergence line persisted there, keeping invigorating the convection (Figure 4g).

Overall, both the large-scale and local conditions were favorable for the development of convection. In particular, the development and maintenance of the quasi-stationary convective system were closely related to the convergence line, which is also found in M. Wu and Luo (2016). However, it is of interest to explore how different factors affected the formation of convergence line, and why the heaviest rainfall occurred near the mountains. Cloud-resolving simulations of this event were conducted to address these questions.

3. Model Configuration and Verification

3.1. Model Configuration

The version of 3.9.1 of Weather Research and Forecasting (WRF) model (Skamarock et al., 2008) was used to simulate this heavy rainfall event. One-way, three nested grids (9/3/1 km) were used with 50 vertical levels. The outermost domain was initialized at 08:00 LST June 21, 2017, and the two inner domains were activated at 14:00 LST June 21, 2017. The integration of all domains ended at 08:00 LST June 22, 2017. The initial and boundary conditions were provided from the ERA-Interim data set with a resolution of 0.75° at 6 h intervals. The following physical schemes were used: RRTMG longwave and shortwave radiation scheme (Iacono et al., 2008), Yonsei University's planetary boundary layer scheme (Hong et al., 2006), Rapid Update Cycle land surface scheme (Benjamin et al., 2004), and National Severe Storms Laboratory two-moment microphysics scheme (Mansell et al., 2010). Grell-Freitas cumulus scheme (Grell & Freitas, 2014) was adopted only in the outermost domain.

In order to investigate the roles of terrain, land-sea roughness contrast, and cold pool outflows on the formation of heavy rainfall, five sensitivity experiments were conducted (Table 1). In these sensitivity experiments, except that some of the above factors were modified, all other configurations were identical to CNTL. For example, to understand the impact of the coastal hills on the formation of the heavy rainfall, the hills near the western coastline of Yangjiang were removed (Exp. NSMT, Figure 7a). Exp. ROU in which surface roughness over the land in the dashed blue rectangle in Figure 8 is set to be the same as that over the sea was designed to test the effect of differential surface roughness during this rainfall event. The influence of convectively generated cold outflows was examined through Exp. NEVP, in which evaporation of rainwater was allowed but no associated evaporative cooling was in the thermodynamic equation.

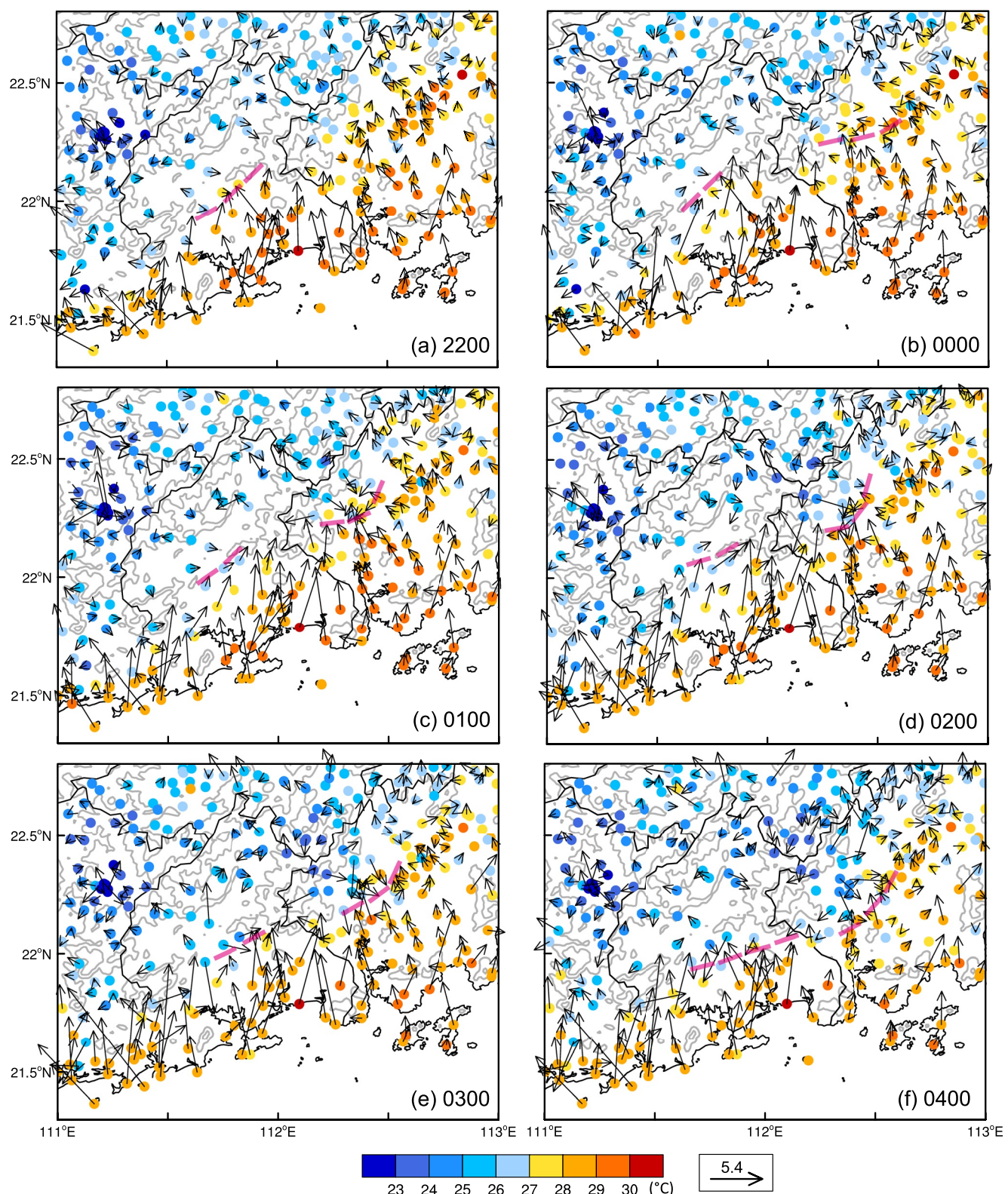


Figure 6. Temperature (colored dots, °C) and winds observed by automatic weather stations at (a) 22:00 LST June 21, (b) 00:00, (c) 01:00, (d) 02:00, (e) 03:00, (f) 04:00 LST June 22, 2017. Dashed pink lines indicate the convergence lines.

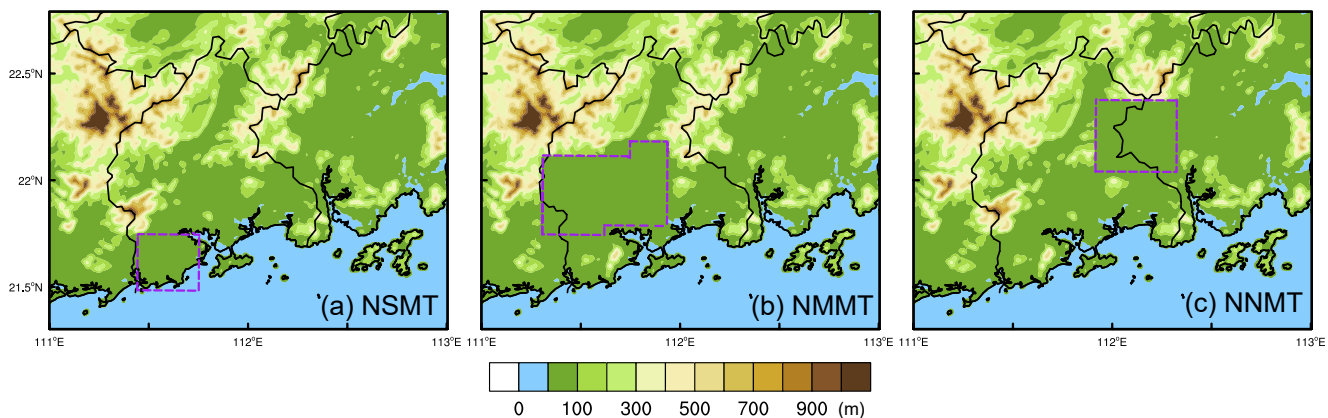


Figure 7. Modified terrain (shaded, m) for Exps. (a) NSMT, (b) NMMT, and (c) NNMT. The modified areas are denoted by dashed purple rectangles.

3.2. Verification of the Control Simulation

The simulated 12 h accumulated precipitation in CNTL (Figure 8) is compared with the observation (Figure 1b). The simulation successfully reproduced the heavy rainfall in the middle of Yangjiang and in the west of Jiangmen, although produced more rainfall near the Maoming-Yangjiang border than the observation. The equitable threat score of the 12 h accumulated precipitation at the 250 mm threshold was 0.6 for CNTL. Figure 9 shows the evolution of simulated composite radar reflectivity. Overall, the initiation and evolution of convective storms

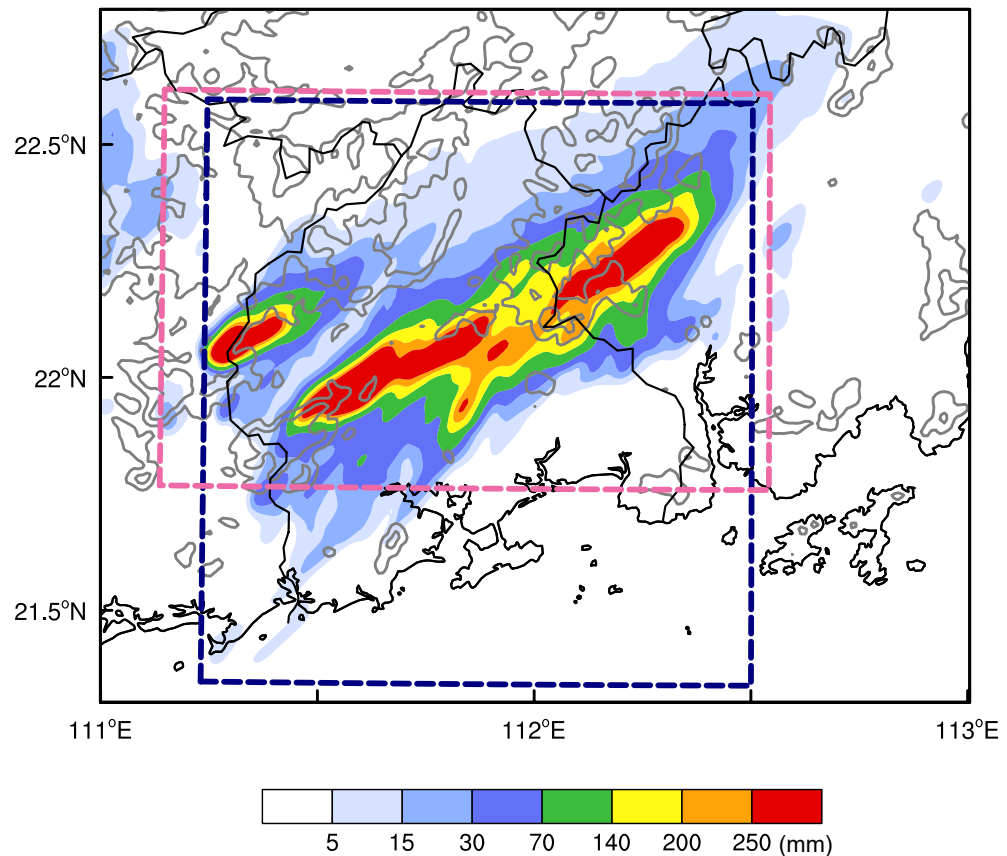


Figure 8. As in Figure 1b, but for the simulated 12 h accumulated rainfall (shaded, mm) for CNTL. The dashed pink rectangle indicates the region for the calculation of water vapor flux (referred to as “region HR” in the text). The dashed blue rectangle denotes the region where the surface roughness over the land is modified in Exp. ROU.

Table 1
Description of Experiment Design

Experiment	Description
CNTL	The control simulation.
NSMT	The mountains near the western coastline of Yangjiang were removed (Figure 7a).
NMMT	The mountains in the middle of Yangjiang were removed (Figure 7b).
NNMT	Part of Mt. Tianlu was removed (Figure 7c).
ROU	The surface roughness over the land in the dashed blue rectangle in Figure 8 was set to be the same as that over the sea.
NEVP	Evaporative cooling was turned off at 01:00 LST June 22, 2017.

were well simulated. As in observation, new convective storms also initiated near coastal hills and the south of Mt. Tianlu, and then moved northeastwards in the simulation (Figures 9a and 9b). Later, a southwest-northeast oriented convective band was formed near Mts. Yunwu and Tianlu around 01:00 LST June 22, and maintained for about 4 h (Figures 9c–9f). After 04:00 LST June 22, the convective band became less connected, and some short convective bands were formed (Figure 9g).

The simulated near-surface winds and temperature are presented in Figure 10. Temperature gradually decreased from the southern coastal area to northern mountainous area. Southerly winds dominated over the sea and coastal area. Winds became weaker inland (Figure 10a). The CNTL reproduced the convergence line in the middle of Yangjiang. Later, as the convective system developed, cold pool outflows were generated and confronted with the southerly flows, enhancing the convergence (Figures 10c and 10d).

To sum up, the CNTL successfully reproduced the evolution of the convective systems and resultant heavy rainfall. CI and the formation of quasi-stationary convective system near mountains were well simulated. The distribution of rainfall, especially heavy rainfall ≥ 250 mm in CNTL also fitted the observation well despite of more elongated shape. The relevant persistent southerly winds near the coastlines and the convergence between warm southerly flows and cold outflows were also captured in the simulation. Therefore, it is reasonable to examine the model results in detail to reveal the roles of different factors in the formation of heavy rainfall.

4. Results of Sensitivity Experiments

4.1. Roles of Terrain

Terrains in different locations might exert different influences on the development of convective storms during this event. Their specific influences are investigated by comparison between CNTL and sensitivity experiments with specific mountains removed. That is, the coastal hills, mountains in the middle of Yangjiang, and part of Mt. Tianlu were removed in Exps. NSMT, NMMT, and NNMT, respectively (Figure 7).

As mentioned in the observational analysis, orographic lifting by the coastal hills and Mt. Tianlu helped to initiate convection at earlier time. The evolution of simulated reflectivity in the sensitivity experiments without some mountains shows that CI near the original locations of mountains was less frequent (Figures 11, 13, and 14), providing evidence that the existence of mountainous terrain assisted CI near the mountains.

CI mostly occurred on the northeast of the coastal hill (Figure 9a). Cross-sections of water vapor, temperature, CIN, and in-plane winds through the coastal hill illustrate the CI process near the coastal hill (Figure 12). The cross-sections for CNTL clearly show that a capping layer with CIN value $\sim 30 \text{ J kg}^{-1}$ existed at around 0.5 km above sea level (ASL) over the ocean on the south of the hill (Figure 12a). A cold region was seen around 0.4–1.3 km ASL over the south side of the hill. Southerly flows along with abundant moisture were lifted by the terrain, leading to condensation. As the cloud moved northwards into the north area of the hill, it developed into stronger convection with additional aid of leeside convergence (Figure 12b). Without the coastal hill (Exp. NSMT), the initial cloud was more difficult to develop, and tended to be restricted below the capping layer (Figure 12c). Total rainfall in the region enclosed by the dashed pink rectangle in Figure 8 (referred to as “region HR” hereafter) in NSMT was $\sim 20\%$ less than that in CNTL (Figure 11c). The difference in the total rainfall between the sensitivity experiment and CNTL can be referred to Figure S1 in Supporting Information S1. In short, the

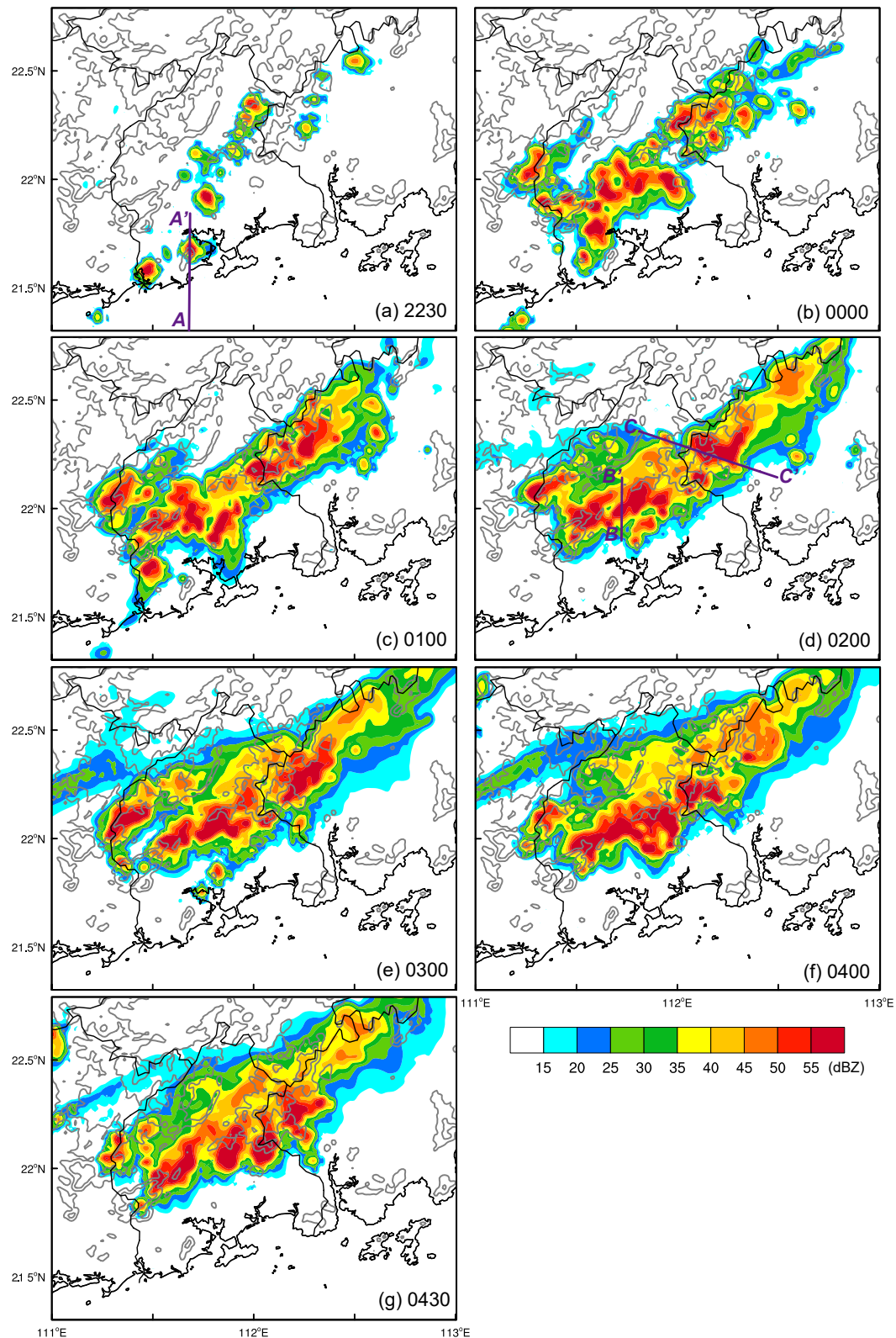


Figure 9. As in Figure 4, but for the simulated composite radar reflectivity (dBZ) for CNTL at (a) 22:30 LST June 21, (b) 00:00, (c) 01:00, (d) 02:00, (e) 03:00, (f) 04:00, and (g) 04:30 LST June 22, 2017. Purple line AA' in (a) marks the location of vertical cross-sections shown in Figure 12. Purple lines BB' and CC' in (d) mark the location of vertical cross-sections shown in Figure 16.

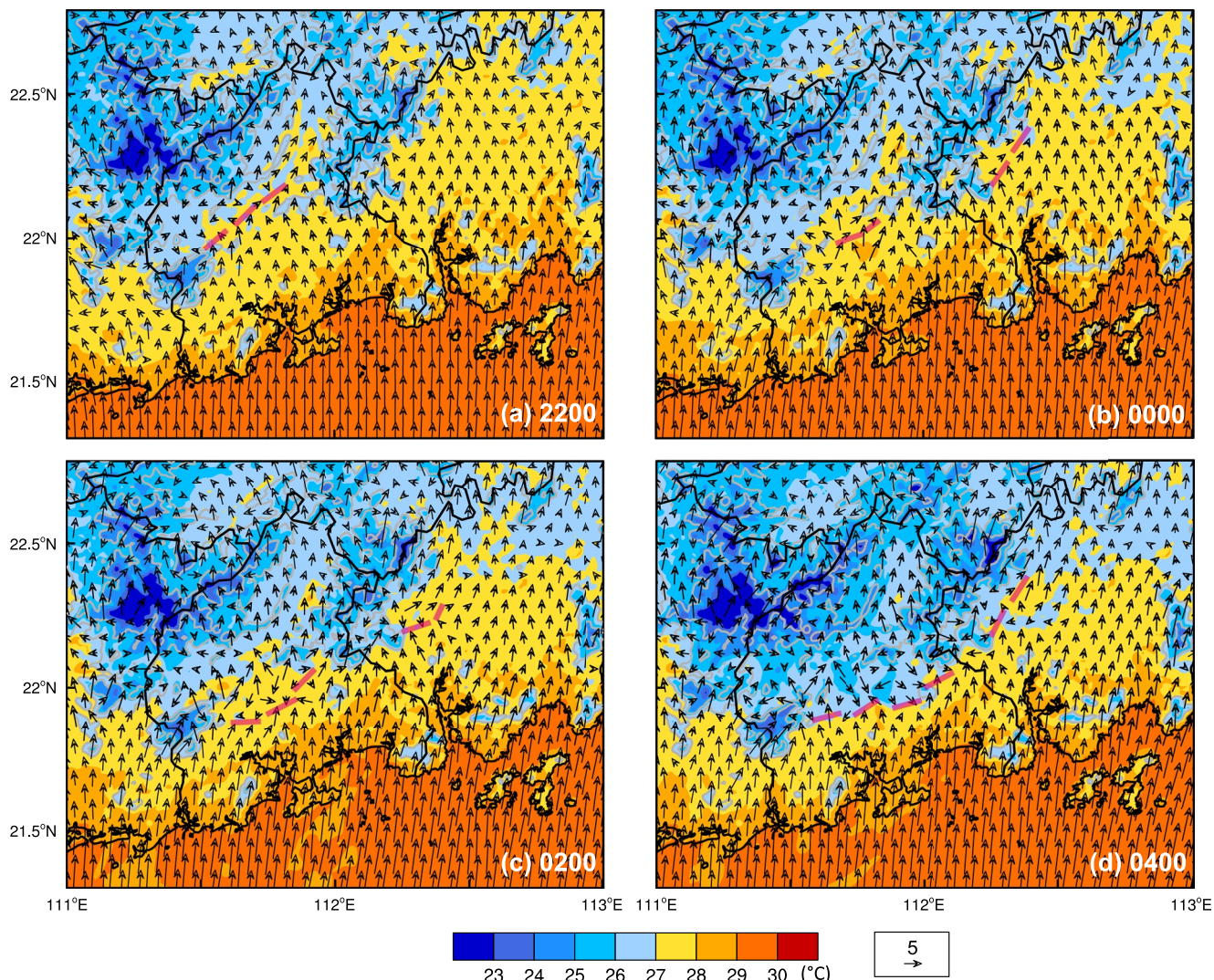


Figure 10. The simulated 2 m temperature (shaded, °C) and 10 m winds for CNTL at (a) 22:00 LST June 21, (b) 00:00, (c) 02:00, and (d) 04:00 LST June 22, 2017. Dashed pink lines indicate the convergence lines.

coastal hill did play a role in lifting moist air. Moreover, the thermal structure of boundary layer over the sea restricted the development of convection and determined that the convection could hardly be initiated until reaching the coastal hills.

Since two centers of heavy rainfall were located near the mountains in the middle of Yangjiang (i.e., the northeast of Mt. Ehuangzhang and the south of Mt. Yunling), it is of interest to examine the influence of these mountains on the formation of heavy rainfall. In NMMT, with these mountains removed (Figure 7b), more convective storms initiated on the south side of Mt. Yunwu, and the storms initiated near the coastline moved fast to the south side of Mt. Yunwu, leading to the formation of a linear convective system near the south side of Mt. Yunwu (Figures 13a and 13b), farther north than the linear convective system in CNTL. Consequently, the heavy rainfall in Yangjiang shifted to farther north (Figure 13c). Figure 13d shows that the southerly winds could penetrate farther inland until they met the northern mountains and turned to be easterly winds. Warm and moist air transported by the southerly winds somewhat counteracted the cooling effect at night on the north of the original Mts. Ehuangzhang and Yunling, which hindered the development of northerly land breeze as well. The low-level temperature on the north of the original Mt. Ehuangzhang was about 1°C warmer in NMMT than that in CNTL, and northerly winds could hardly be found there in NMMT. It is also noticed that the near surface winds became weaker over the modified terrain (i.e., the original location of Mts. Ehuangzhang and Yunling) in NMMT compared with

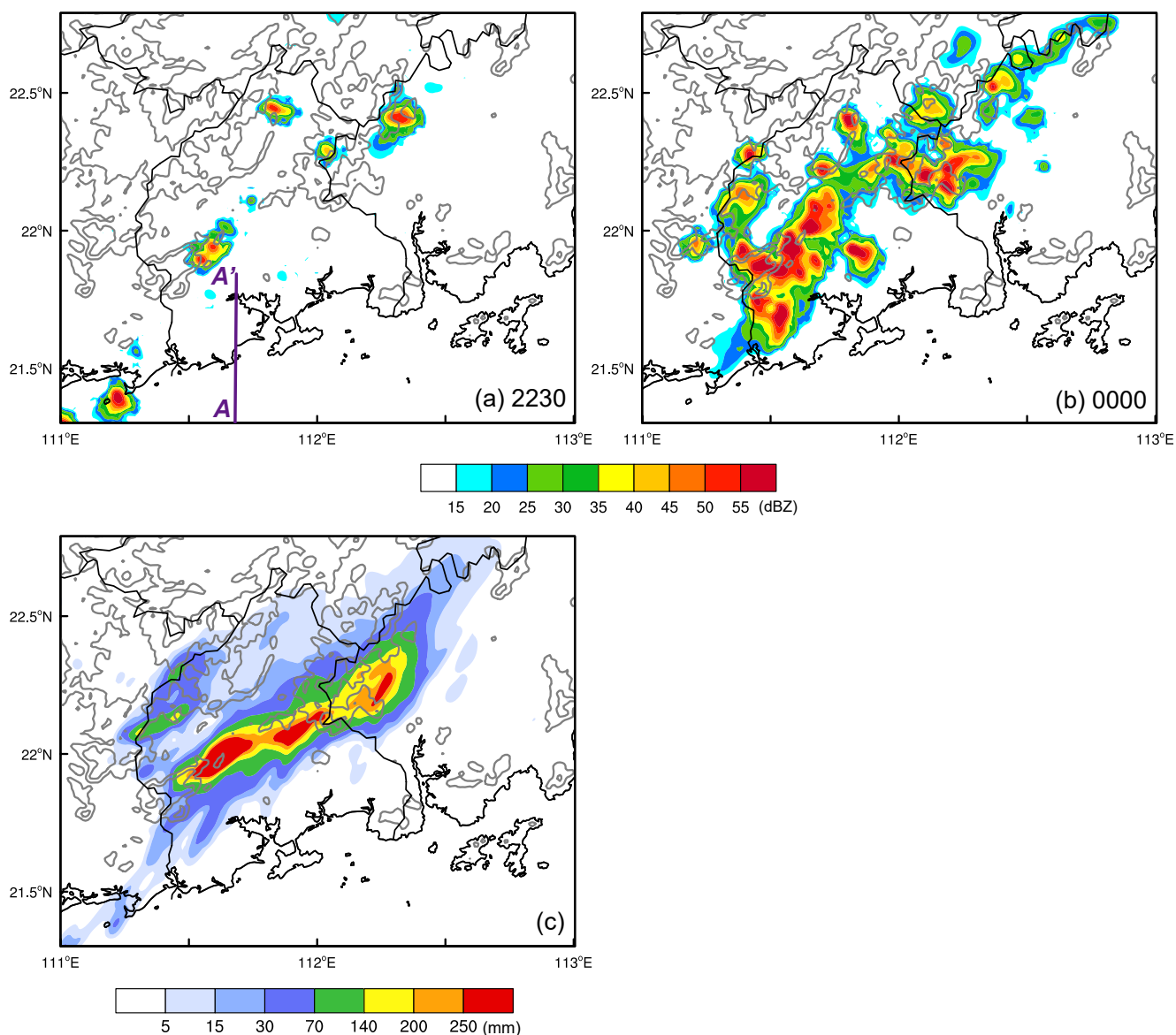


Figure 11. The simulated radar reflectivity for Exp. NSMT at (a) 22:30 LST June 21, and (b) 00:00 LST June 22, 2017. Line AA' in (a) shows the same location as that in Figure 9a. (c) As in Figure 1b, but for the simulated 12 h accumulated rainfall (shaded, mm) for Exp. NSMT.

those in CNTL. This is because in CNTL, in the presence of Mts. Ehuangzhang and Yunling, the near-surface winds over the mountains were at a high elevation with fewer obstructions (e.g., buildings) around them at the same elevation, and thus the winds were close to the environment winds at the same elevation which are usually stronger than those at a lower elevation.

Comparison between NMMT and CNTL demonstrates that the mountains in the middle of Yangjiang contributed to the formation of the convergence line and obstructing the northward movement of the convective storms.

In NNMT, after removing part of Mt. Tianlu (Figure 7c), convective storms and associated rainfall near Yangjiang-Jiangmen border was notably reduced (Figures 14a–14c). The total rainfall in the region HR was ~17% less than CNTL. In the absence of Mt. Tianlu, the low-level winds turned to be more uniform near Yangjiang-Jiangmen border, and the convergence was weaker than that in CNTL. This difference between NNMT and CNTL was more distinct when cold pool outflows strengthened (Figure 14d). The westward concave morphology of Mt. Tianlu complicated the wind direction near Mt. Tianlu, resulting in favorable local convergence under the synoptic situation of this event.

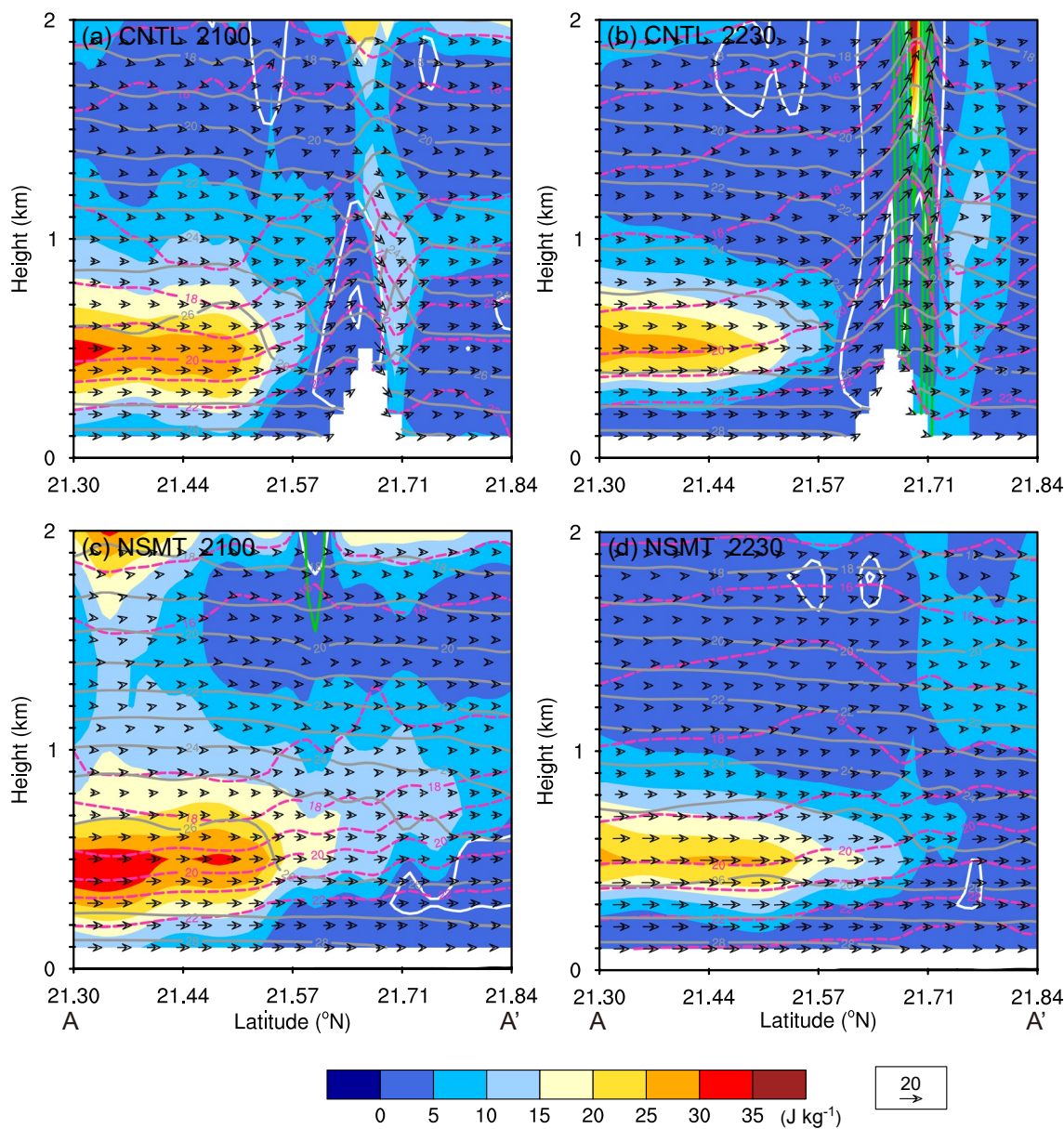


Figure 12. Vertical cross-sections along the line AA' given in Figures 9a and 11a of CIN (shaded, J kg^{-1}), temperature (contoured in solid gray at intervals of 1°C), water vapor (contoured in dashed maroon at intervals of 1 g kg^{-1}), cloud water (contoured in white starting at 0.1 g kg^{-1} at intervals of 1 g kg^{-1}), and rainwater (contoured in green starting at 0.1 g kg^{-1} at intervals of 1 g kg^{-1}), superimposed with in-plane vectors with vertical motion amplified by a factor of 10 for (a, b) CNTL, and (c, d) Exp. NSMT at 21:00 (left column), and 22:30 LST (right column) June 21.

In order to further explore the importance of the small-scale terrain features on the formation of heavy rainfall, an additional experiment was conducted using terrain data with a coarser resolution (Figure S2a in Supporting Information S1). That is, the same model configurations were adopted as CNTL, but terrain data with a 2-arcmin resolution were used in this sensitivity experiment instead of that with a 30-arcsec resolution in CNTL. The 12 h accumulated precipitation in this experiment was overall weaker than that in CNTL, especially the area of heavy rainfall $\geq 250 \text{ mm}$ near Mt. Tianlu much smaller (Figure S2b in Supporting Information S1). Fewer local convergence zones were found near Mt. Tianlu due to more uniform winds near the smoother terrain, which could account for less CI and rainfall near the mountains. In addition, it suggests that detailed representation of the terrain features is essential for predicting heavy rainfall over this mountainous coastal region.

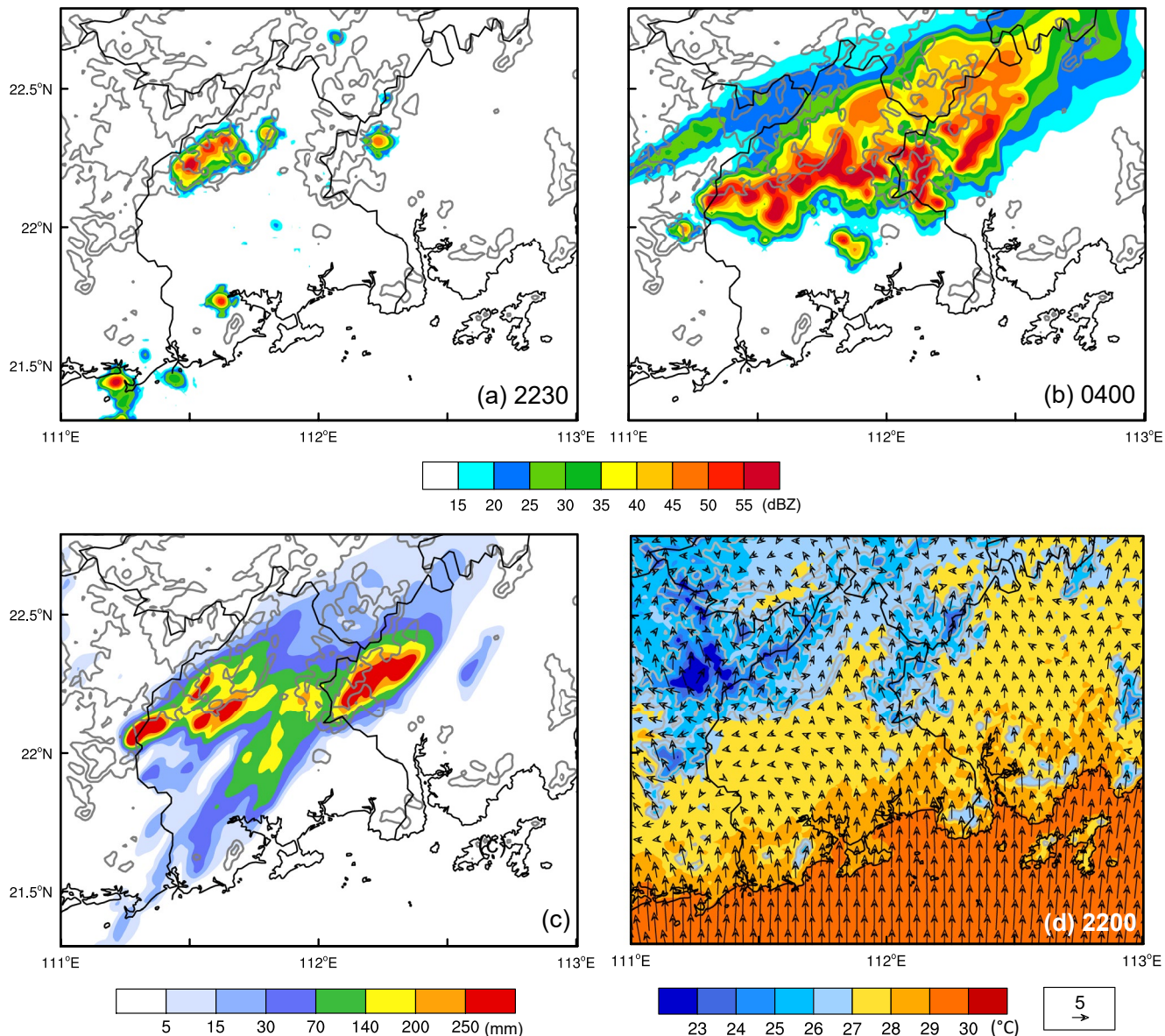


Figure 13. The simulated radar reflectivity for Exp. NMMT at (a) 22:30 LST June 21, and (b) 04:00 LST June 22, 2017. (c) As in Figure 11c but for Exp. NMMT. (d) As in Figure 10a but for Exp. NMMT.

4.2. Role of Surface Roughness

Besides the orographic effects, the convergence line in the middle of Yangjiang was found to be crucial to the development of convective storms. The convergence line was formed by the weak winds over the northern mountainous area and relatively strong southerly winds near the coast. It is hypothesized that land-sea surface roughness contrast can be one of the causes affecting the formation of convergence line. In most previous studies on the impact of land-sea contrast on the development of convection over South China, they conducted sensitivity experiments with the coastal land replaced by ocean, and mixed up the roles of land-sea thermal and surface roughness contrasts (e.g., Du, Chen, Han, Mai, et al., 2020). In the present study, to examine the role of surface roughness, the surface roughness over the land in the dashed blue rectangle shown in Figure 8 was reduced to be the same as that over the sea (Exp. ROU). Low-level winds in ROU are compared with those in CNTL. As the surface roughness was reduced over the land in ROU, the southerly winds were less weakened over the land, and could intrude further inland than those in CNTL (Figure 15d). As a result, the convergence line did not form in the middle of Yangjiang.

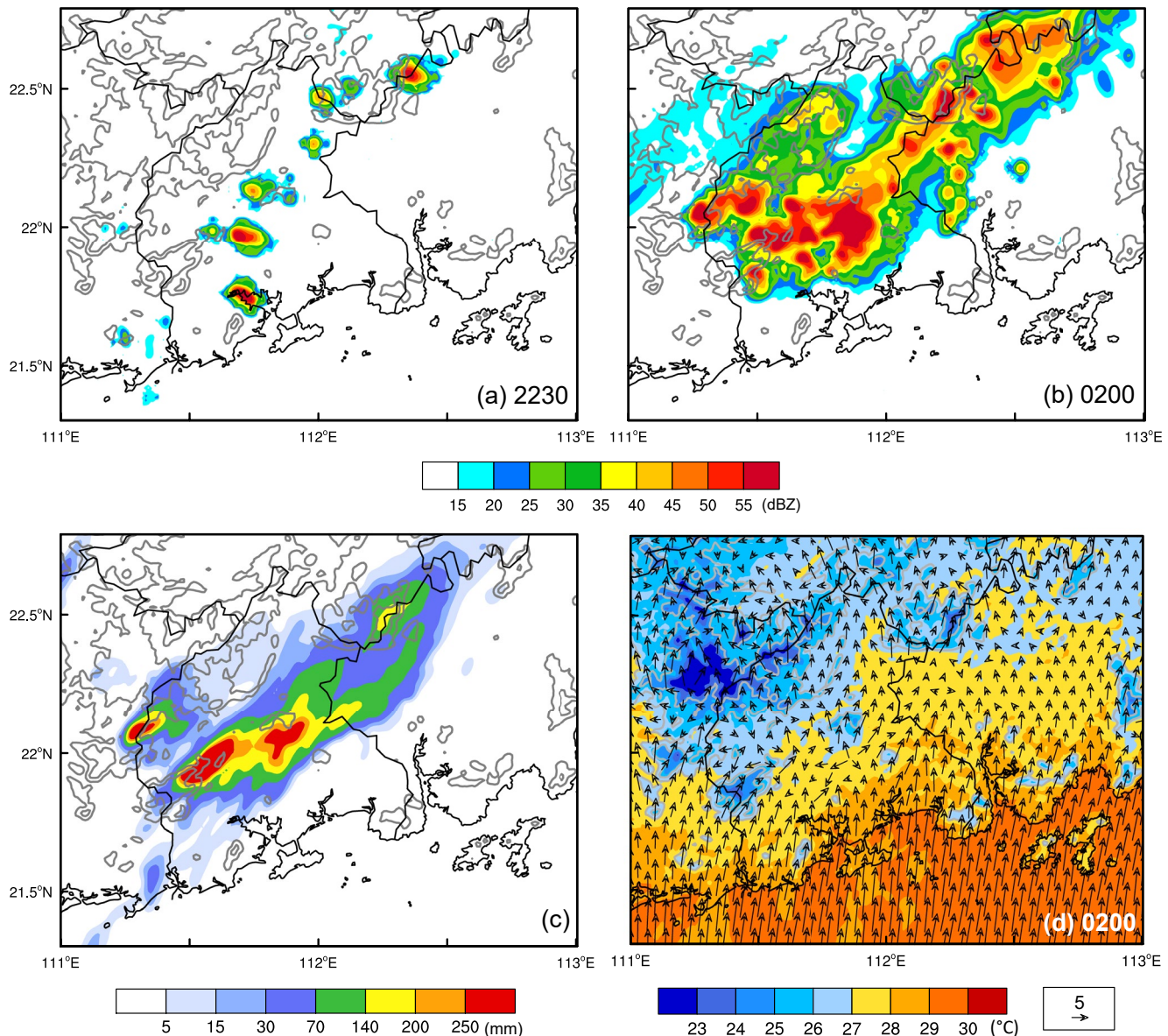


Figure 14. The simulated radar reflectivity for Exp. NNMT at (a) 22:30 LST June 21, and (b) 02:00 LST June 22, 2017. (d) As in Figure 11c but for Exp. NNMT. (c) As in Figure 10c but for Exp. NNMT.

Since the convergence also influenced the moisture supply for heavy rainfall, the water vapor flux across the four boundary surfaces surrounding the region HR was calculated by:

$$Q\text{Flux} = \oint_s \rho Q_v V_n d\sigma, \quad (1)$$

where ρ is air density, Q_v is mixing ratio of water vapor, V_n is wind component perpendicular to each surface (positive values indicate inward direction), and $d\sigma$ is an element on the surface. Figure 16a shows water vapor flux (solid lines) together with area-averaged accumulated rainfall (dashed lines) within the region HR at 1 h intervals. The temporal variation of both water vapor flux and rainfall was similar in CNTL and ROU. Rainfall sharply increased from 23:00 LST June 21, and increase in water vapor flux occurred about 1 h earlier than that in rainfall. Water vapor flux and hourly rainfall in ROU were overall less than those in CNTL. The general decline in rainfall appeared earlier in ROU than that in CNTL. Vertical distribution of water vapor flux further shows that the most distinct inward water vapor was found around 0.5 and 2 km ASL in both CNTL and ROU (Figures 16b and 16c). Maximum water vapor flux in CNTL was greater than that in ROU by ~6%. Negative water vapor flux appeared

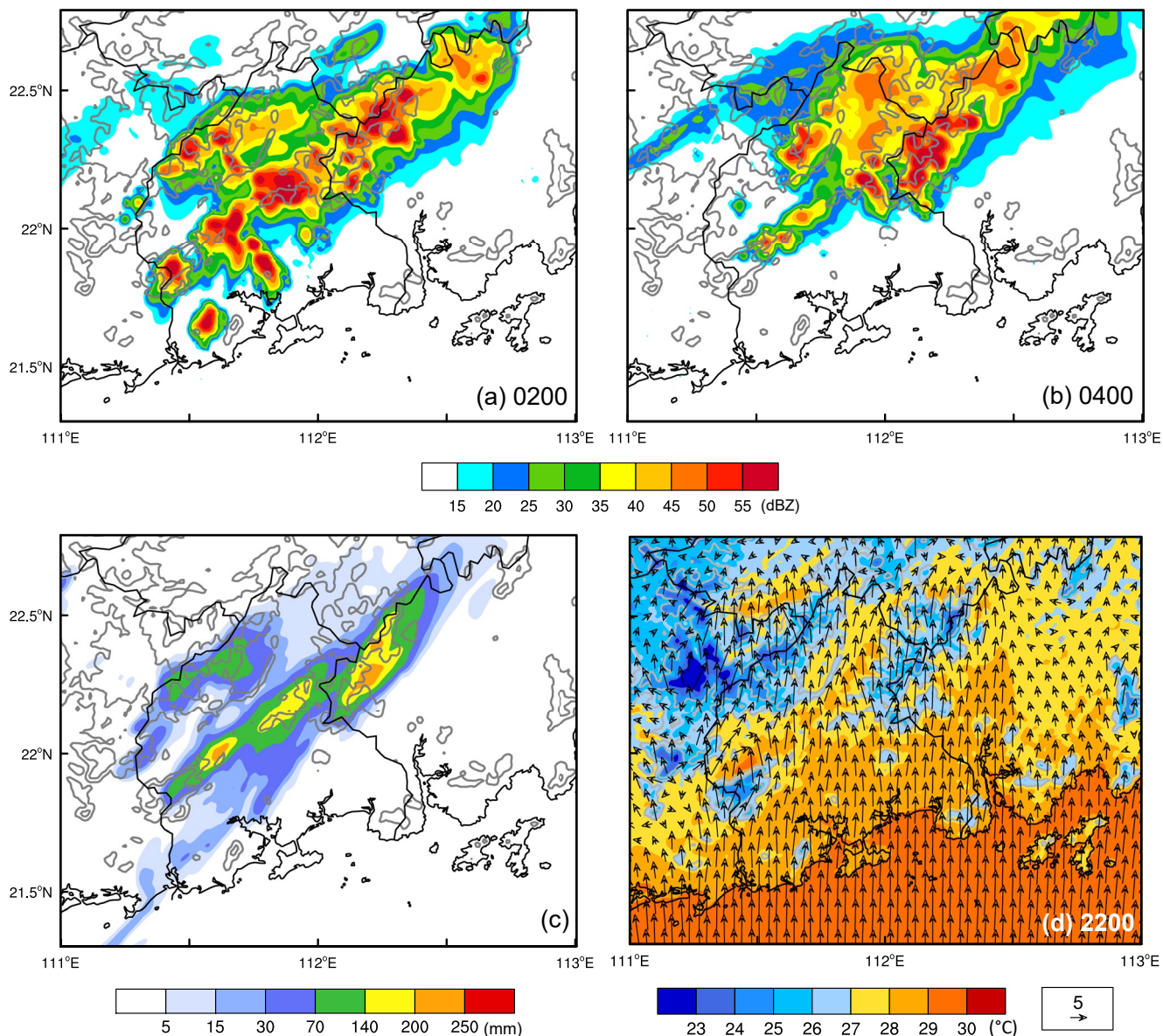


Figure 15. The simulated radar reflectivity for Exp. ROU at (a) 02:00, and (b) 04:00 LST June 22, 2017. (d) As in Figure 11c but for Exp. ROU. (c) As in Figure 10a but for Exp. ROU.

below 1 km and around 3 km after 03:00 LST June 22 in ROU, earlier than that in CNTL, which was consistent with the earlier decline in rainfall in ROU.

Without the support of convergence line in terms of dynamic effect as well as moisture accumulation, convective storms were difficult to maintain over the middle of Yangjiang, and quickly moved out of the region (Figures 15a and 15b), leading to less accumulated rainfall and earlier end of rainfall (Figure 15c). On the whole, the total rainfall in the region HR was markedly reduced by ~44% compared with CNTL. This further confirms that the convergence line was of vital importance to the formation of heavy rainfall.

4.3. Role of Cold Pool Outflows

Northerly outflows associated with the cold pools generated by the convective systems also played a role in sustaining the convection development during the later period through converging with the environmental southerly flows, especially in the east of Mt. Tianlu. If the evaporative cooling was turned off just after the formation of

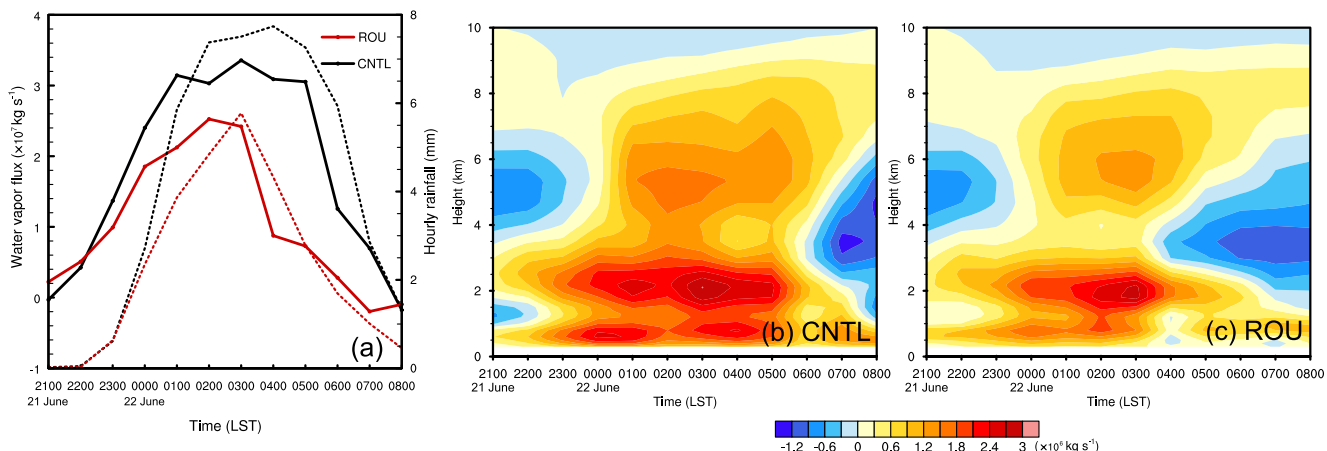


Figure 16. Temporal variation of (a) total water vapor flux (solid lines, kg s^{-1}) and area-averaged hourly rainfall (dashed lines, mm) for CNTL (black) and ROU (red), and vertical distribution of water vapor flux for (b) CNTL and (c) ROU within the dashed pink rectangle in Figure 8 from 21:00 LST June 21 to 08:00 LST June 22. The x-axis labels denote the ending time of hourly rainfall.

the convective band at 01:00 LST June 22 (Exp. NEVP), southerly flows would dominate over Yangjiang and Jiangmen even in the later period in NEVP (Figure 17d) rather than the expansion of northerly outflows in CNTL (Figures 10c and 10d). In the absence of the convergence between northerly outflows and southerly flows, the convective storms moved northwards faster until they were blocked by the northern mountains. A convective band was formed between Mts. Yunwu and Tianlu around 03:00 LST June 22 (Figure 17a), but gradually dissipated 1 h later (Figure 17b). Correspondingly, a distinct rainfall band was formed over there in NEVP (Figure 17c), which did not appear in CNTL, and rainfall over the middle of Yangjiang and the east of Mt. Tianlu was much reduced compared with CNTL. Total rainfall in the region HR in NEVP was $\sim 33\%$ less than that in CNTL. In short, cold northerly outflows helped to maintain the convergence line and the associated convective system in the middle of Yangjiang and the east of Mt. Tianlu during the later period, favoring the continuous production of rainfall over this area.

Vertical cross-sections of reflectivity, divergence, and cold pool height passing through the intense convective storms in the middle of Yangjiang (Line BB' in Figure 9d) and near Mt. Tianlu (Line CC' in Figure 9d) are shown in Figure 18. The depth of the cold pool is defined as the height at which perturbation virtual potential temperature (θ_v') first exceeds -1 K . Virtual potential temperature (θ_v) is calculated by:

$$\theta_v = \theta(1 + 0.608q_v - q_c - q_r), \quad (2)$$

where θ is potential temperature, and q_v , q_c , and q_r are mixing ratio of water vapor, cloud water, and rainwater, respectively. θ_v' is defined as departure from the domain-average of θ_v . Figure 18a shows that convectively generated outflows and southerly flows sustained low-level convergence near 21.93°N at 02:00 LST June 22. At 03:00 LST, while low-level convergence still existed, enhanced convergence was produced in the middle levels due to latent heating, inducing strong upward motion greater than 20 m s^{-1} (Figure 18b). As for the cross-section near Mt. Tianlu (Figure 18e), a notable cold pool with a depth of $\sim 2 \text{ km}$ was generated under the intense convective storm in CNTL. The outflows associated with the cold pool converged with southeasterly flows, and thus enhanced the upward motion ahead of the cold pool, which was beneficial to the continuous development of convection. The combined effects of cold pool and environmental conditions favored the development of convection (Rotunno et al., 1988). At 03:00 LST, intense convection moved slightly eastwards (Figure 18f). Although the cold pool was shallow at that time, convergence between outflows and southeasterly flows was distinct, and so did upward motion. In the cross-sections from NEVP (Figures 18c, 18d, 18g, and 18h), the cold pool was hardly found, and southerly southeasterly flows dominated in the low levels. Convergence was comparatively shallow and upward motion in the area with intense convection was weaker than that in CNTL. Consequently, intense convection could not maintain in the middle of Yangjiang or near Mt. Tianlu in NEVP as long as that in CNTL.

To further compare the effects of different factors, hourly rainfall averaged over the region HR for CNTL and five sensitivity experiments are displayed in Figure 19. The reduction in ROU and NEVP was most significant. The

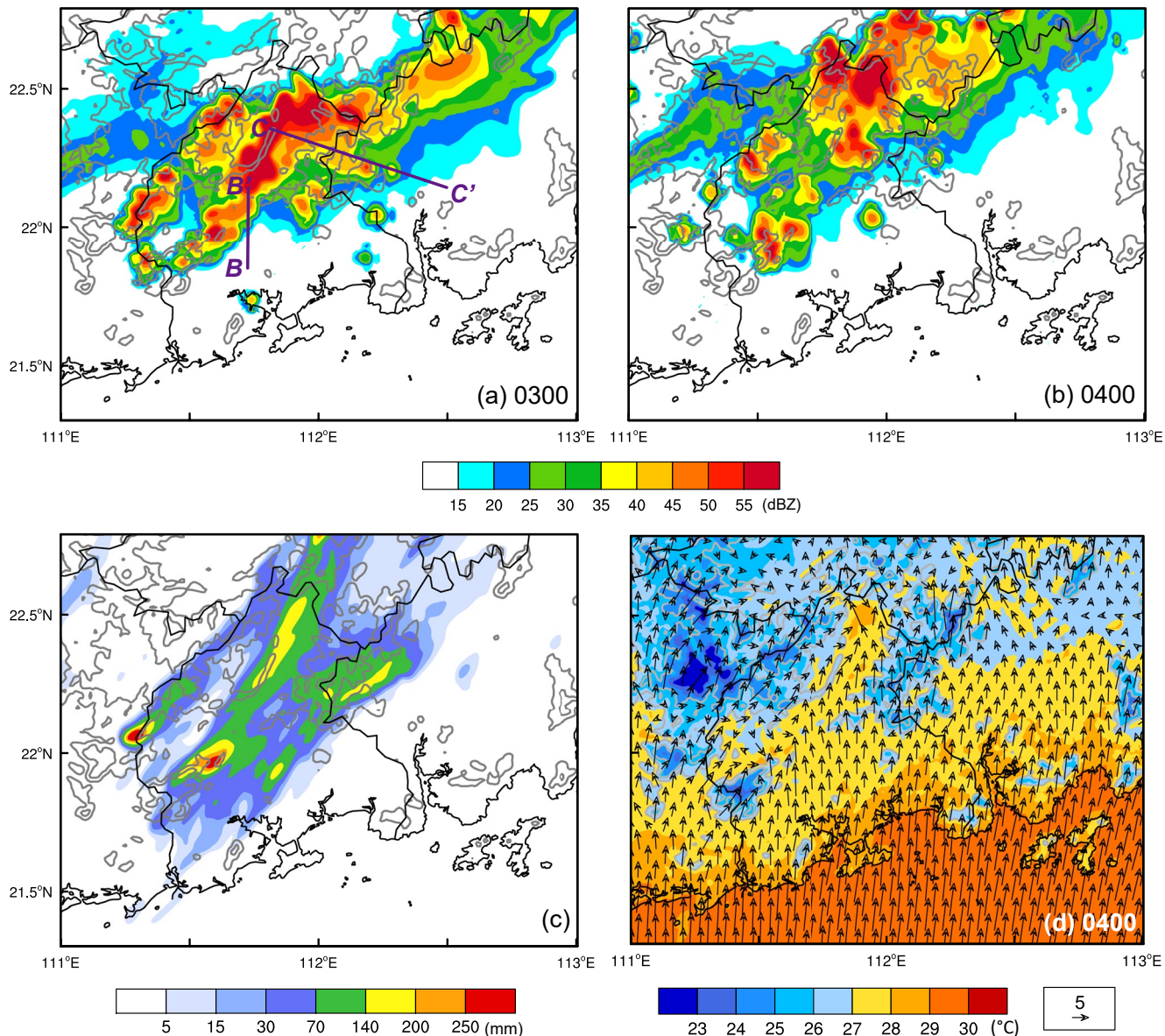


Figure 17. The simulated radar reflectivity for Exp. NEVP at (a) 03:00, and (b) 04:00 LST June 22, 2017. (d) As in Figure 11c but for Exp. NEVP. (c) As in Figure 10d but for Exp. NEVP.

start time of rainfall was similar in all the experiments, but the peak time (i.e., time with the maximum hourly rainfall) and decrease appeared earlier in the sensitivity experiments than that in CNTL. The decrease in rainfall appeared earliest in NEVP, indicating the indispensable role of convectively generated cold pool outflows in the maintenance of the precipitation system.

4.4. Ensemble Analysis

The impacts of different factors evaluated by a deterministic forecast may involve uncertainties associated with the initial conditions and boundary conditions (e.g., Berner et al., 2011; Hamill & Colucci, 1997; Schwartz et al., 2010; Zhuang et al., 2021). An ensemble method can help filter out some uncertain signals. In order to consolidate the conclusions drawn from the above deterministic experiments, a set of ten-member ensemble simulations were produced with initial conditions and boundary conditions perturbations introduced. The corresponding

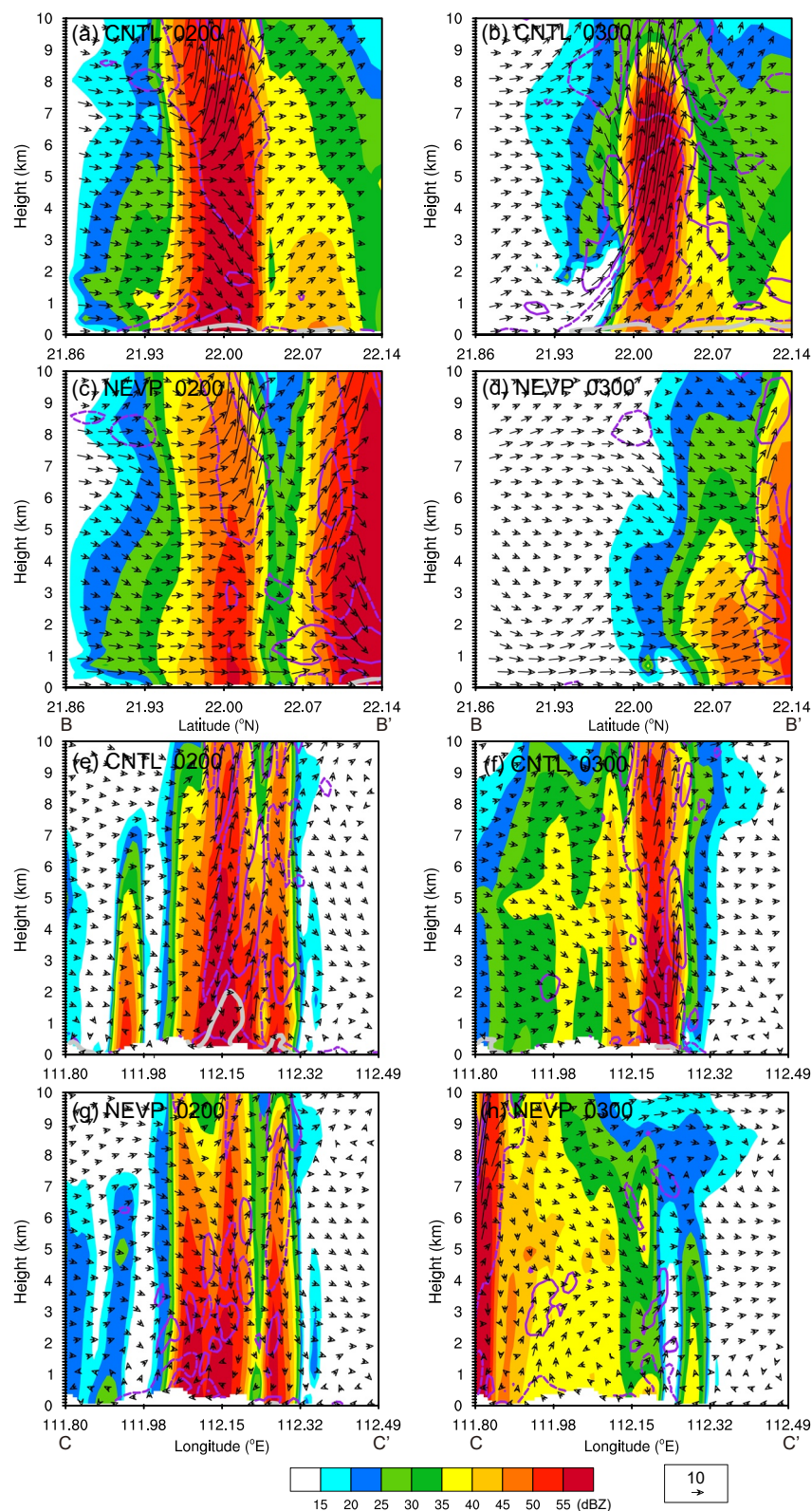


Figure 18. Vertical cross-sections along the lines BB' (a–d) and CC' (e–h) given in Figures 9d and 17a of reflectivity (shaded, dBZ), divergence (dashed purple contours for -5×10^{-4} , $-1 \times 10^{-4} \text{ s}^{-1}$, and solid purple contours for 5×10^{-4} , $1 \times 10^{-4} \text{ s}^{-1}$), and cold pool height (gray contours), superimposed with in-plane vectors with vertical motion amplified by a factor of 5 for CNTL (first and third rows), and Exp. NEVP (second and fourth rows) at 02:00 (left column), and 03:00 LST (right column) June 22.

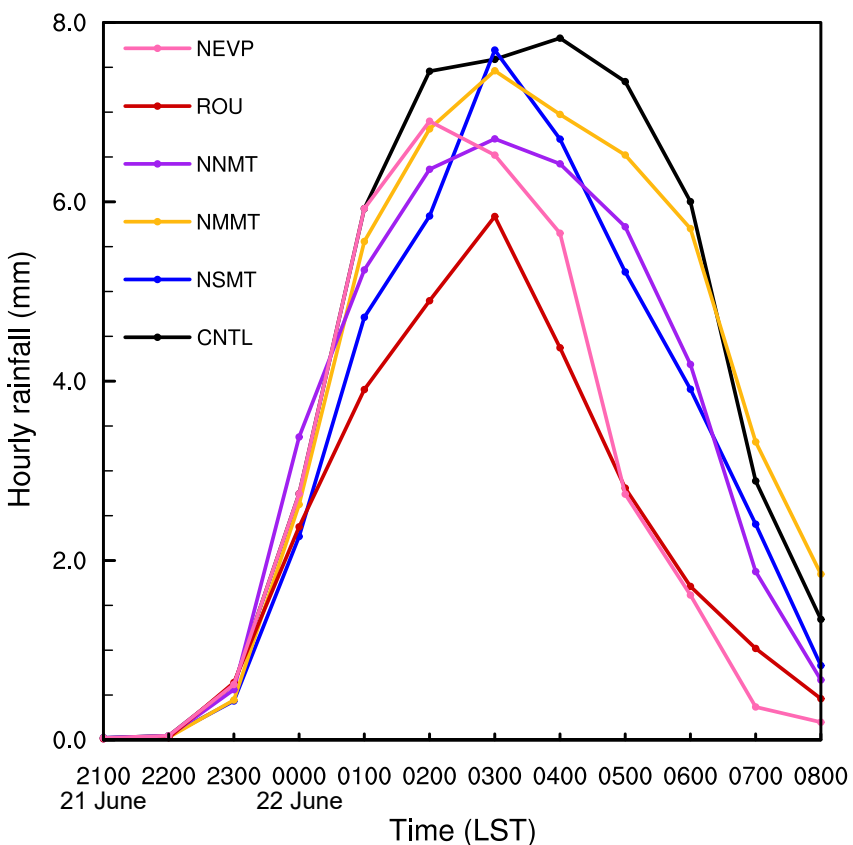


Figure 19. Temporal variation of area-averaged hourly rainfall over the dashed pink rectangle in Figure 8 for CNTL (black), NSMT (blue), NMNM (gold), NNMT (purple), ROU (red), and NEVP (pink) from 21:00 LST June 21 to 08:00 LST June 22.

NSMT, NMNM, NNMT, ROU, NEVP experiments (Table 1) were performed based on each ensemble member. Other model configurations were identical to the CNTL.

The ensemble mean 12 h accumulated rainfall also presents the centers of heavy rainfall in the middle of Yangjiang and in the west of Jiangmen albeit with smaller amounts (Figure 20a). It implies that even slight uncertainty in the initial and boundary conditions can result in perceptible differences in the rainfall forecast. The ensemble simulations for the sensitivity experiments show that without the coastal hills, total rainfall in the region HR was reduced by ~3% (Figure 20b). Without the mountains in the middle of Yangjiang, the heavy rainfall in Yangjiang was located to farther north (Figure 20c). With part of Mt. Tianlu removed, the heavy rainfall center in the west of Jiangmen diminished (Figure 20d). When the surface roughness over the land was reduced, or the evaporative cooling was restricted, the convergence line was weakened and the rainfall in the region HR was much reduced by ~43% in ROU and ~23% in NEVP, respectively (Figures 20e and 20f). The drastic reduction in ROU from both deterministic and ensemble experiments further indicates the vital role of land-sea surface roughness contrast in the formation of heavy rainfall during this event. The results from each ensemble member are displayed in Figure S3 in Supporting Information S1. In terms of the differences between the sensitivity experiments and the control simulation, each ensemble member shows similar results to the deterministic experiments and the ensemble mean.

In general, the impacts of terrain, land-sea surface roughness contrast, and cold pool outflows on the rainfall based on the ensemble experiments are consistent with the conclusions drawn from the deterministic experiments, although the specific values of the difference in the ensemble mean rainfall between the control simulations and the corresponding sensitivity experiments are not equal to those calculated from the deterministic experiments.

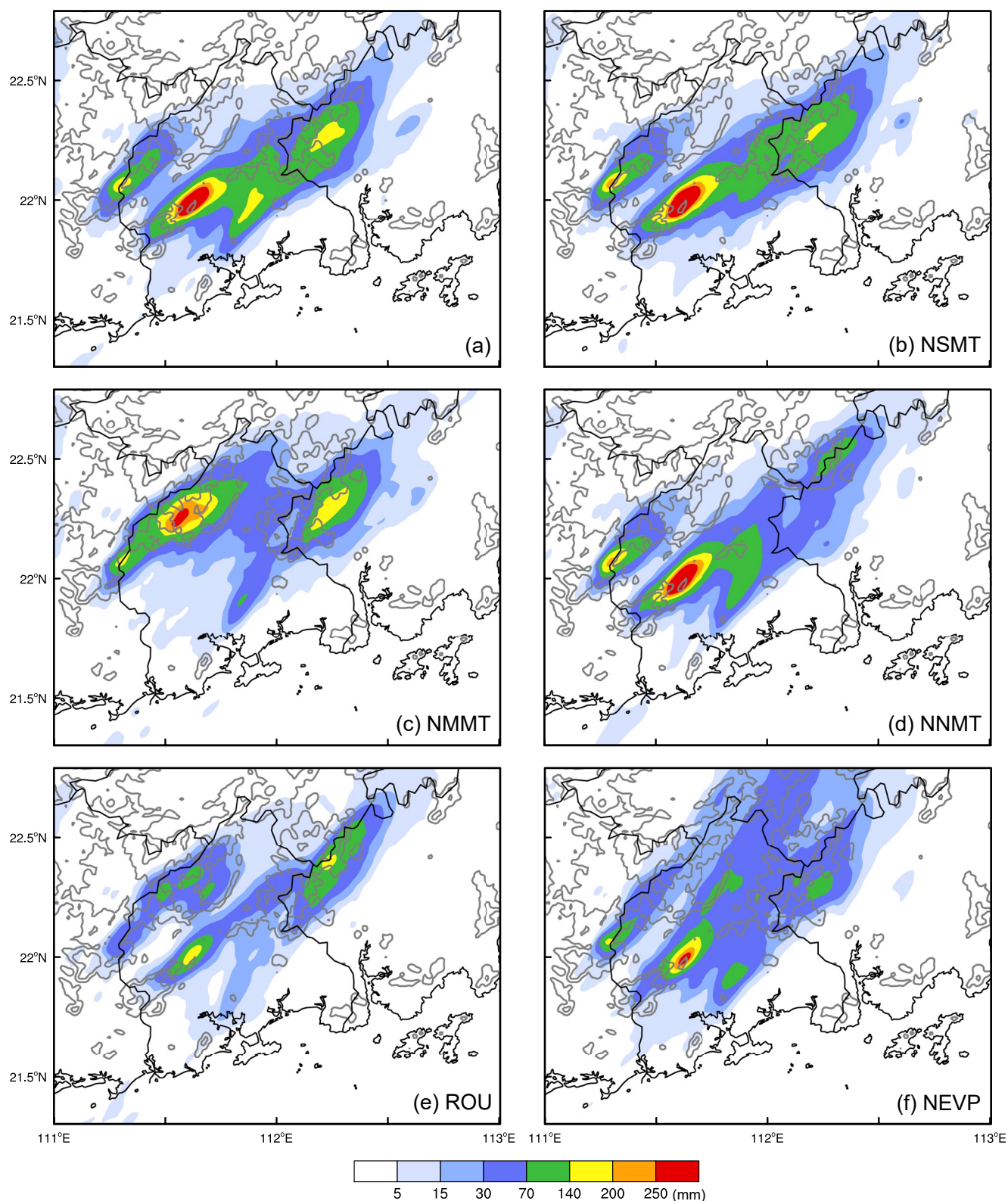


Figure 20. As in Figure 8 but for the ensemble mean of (a) the control simulations, (b) NSMT, (c) NMMT, (d) NNMT, (e) ROU, and (f) NEVP experiments.

5. Summary and Conclusions

Using observations and numerical simulations, the formation of extremely heavy rainfall produced by a quasi-stationary mesoscale convective system over the western coastal region of South China during June 21–22, 2017 is investigated. The influences of terrain, land-sea surface roughness contrast, and cold pool outflows on the development of convection and associated rainfall are examined through a series of sensitivity experiments.

Synoptic analysis shows that southerly winds continually conveyed warm, moist air to South China. After midnight, low-level jet originating from the South China Sea extended to the land, enhancing boundary-layer convergence near the coastal region. Thermodynamic environmental conditions including small CIN, low LCL and LFC, and large CAPE were favorable for the development of convective storms.

Initial convective storms developed in the northeast of Mt. Longgao near the coastline, the windward side of Mt. Tianlu, or the middle of Yangjiang. A quasi-stationary convergence line between weak cold northerly winds and strong warm southerly flows was formed in the middle of Yangjiang and the west of Jiangmen, which played a crucial role in supporting the development, organization and maintenance of convective storms, similar to the extreme rainfall case studied in Huang, Liu, Liu, Li, and Knievel (2019). The convective storms moved north-eastwards and were organized along the convergence line into a linear convective system. The linear convective system maintained near the convergence line for about 4 h, continuously dropping rain over Yangjiang and Jiangmen. Cold pool outflows associated with the convective system continued to converge with the southerly flows, sustaining the convergence and thus the maintenance of the linear convective system.

A series of high-resolution simulations was performed using the WRF model to further examine the roles of terrain, land-sea surface roughness contrast, and cold pool outflows in the formation of the heavy rainfall. The CNTL successfully reproduced the evolution of convection and the distribution of heavy rainfall. A sensitivity experiment with hills near the coastline removed shows that CI occurred less frequently near these hills. Besides the orographic lifting effect, the coastal hills also acted to reduce the stability, facilitating the development of shallow clouds to deep convection near the coast. When the mountains in the middle of Yangjiang (farther from the coastline) were removed, more convection initiated near the south side of the northern mountains. The convergence line became unclear over the middle of Yangjiang. As a result, a linear convective system maintained near the south foot of the northern mountains instead of the middle of Yangjiang. Centers of heavy rainfall shifted to farther north. The mountains in the middle of Yangjiang not only directly lifted the warm moist air to achieve CI, but also affected the formation of convergence line and the movement of convection. As for Mt. Tianlu, it facilitated the lifting of impinging flows and the formation of local convergence. With Mt. Tianlu removed, heavy rainfall near Mt. Tianlu became less distinct, and the total rainfall in the region of interest was reduced.

The vital role of the differential surface roughness between land and sea in the formation of the convergence line was illustrated by a sensitivity experiment where the surface roughness over the land was reduced. The convergence line could not form and the net moisture flux was reduced in this experiment, leading to less accumulated rainfall.

During the later period of this event, the cold pool outflows converged with the ambient southerly flows, supporting the maintenance of convergence and associated linear convective system. When the evaporative cooling was turned off, the convective storms quickly moved farther north, and consequently a relatively weak rainfall band was formed farther north.

Coastal regions are characterized by heterogeneous underlying surface, which leads to the various and complicated distribution of low-level winds, temperature, and moisture, greatly challenging accurate weather forecasts. This study suggests that it is important to capture the persistent strong southerly winds (both speed and direction) over the land near the coastline and over the adjacent sea, and the quasi-stationary mesoscale boundary (a convergence line as well as a thermal boundary) formed under the combined influence of synoptic flows, terrain, land-sea contrast, and cold pools for the prediction of heavy rainfall over the coastal region of South China in this event. The experiments using other analysis datasets (including ERA5, GFS, FNL, and CFSR) as initial and boundary conditions were also run. The initial fields provided by these analysis datasets show some differences in moisture, temperature, winds, etc. Results show that low-level winds in Yangjiang near the coastline and over the sea turned to be more southwesterly after 22:30 LST June 21, and lifting by the mountains in the middle of Yangjiang and the convergence line was less distinct in those experiments than that in CNTL. Consequently, most

heavy rainfall fell in the west of Jiangmen, and heavy rainfall in the middle of Yangjiang was missing in those experiments (Figure S4 in Supporting Information S1).

In the ongoing work, the cloud microphysical characteristics and processes associated with extreme hourly rainfall of 165 mm are further explored by both observational analysis and process-based modeling study, and they will be compared with the record-breaking rainfall event studied in Huang et al. (2020).

Data Availability Statement

The data in this study has been archived at the Harvard data server (<https://doi.org/10.7910/DVN/YR0S65>).

Acknowledgments

This work was supported by the National Natural Science Foundation of China (41905047, 42030610), the Open Research Program of the State Key Laboratory of Severe Weather (2019LASW-B03), the Guangdong Basic and Applied Basic Research Foundation (2021A1515011415), and the National Natural Science Foundation of China (42075014). The authors are grateful to the European Centre for Medium-Range Weather Forecasts (ECMWF) for providing ERA-Interim data (<https://apps.ecmwf.int/datasets/data/interim-full-daily/>).

References

- Arritt, R. W. (1993). Effects of the large-scale flow on characteristic features of the sea breeze. *Journal of Applied Meteorology and Climatology*, 32, 116–125. [https://doi.org/10.1175/1520-0450\(1993\)032<0116:EOTLSF>2.0.CO;2](https://doi.org/10.1175/1520-0450(1993)032<0116:EOTLSF>2.0.CO;2)
- Bai, L., Chen, G., & Huang, L. (2020). Convection initiation in monsoon coastal areas (South China). *Geophysical Research Letters*, 47, e2020GL087035. <https://doi.org/10.1029/2020GL087035>
- Baker, R. D., Lynn, B. H., Boone, A., Tao, W. K., & Simpson, J. (2001). The influence of soil moisture, coastline curvature, and land-breeze circulations on sea-breeze-initiated precipitation. *Journal of Hydrometeorology*, 2, 193–211. [https://doi.org/10.1175/1525-7541\(2001\)002<0193:TISMC>2.0.CO;2](https://doi.org/10.1175/1525-7541(2001)002<0193:TISMC>2.0.CO;2)
- Barthlott, C., & Kirshbaum, D. J. (2013). Sensitivity of deep convection to terrain forcing over Mediterranean islands. *Quarterly Journal of the Royal Meteorological Society*, 139, 1762–1779. <https://doi.org/10.1002/qj.2089>
- Benjamin, S. G., Grell, G. A., Brown, J. M., Smirnova, T. G., & Bleck, R. (2004). Mesoscale weather prediction with the RUC hybrid isentropic-terrain-following-coordinate model. *Monthly Weather Review*, 132, 473–494. [https://doi.org/10.1175/1520-0493\(2004\)132<0473:mwpwtr>2.0.co;2](https://doi.org/10.1175/1520-0493(2004)132<0473:mwpwtr>2.0.co;2)
- Bennett, L. J., Blyth, A. M., Burton, R. R., Gadian, A. M., Weckwerth, T. M., Behrendt, A., et al. (2011). Initiation of convection over the Black Forest mountains during COPS IOP 15a. *Quarterly Journal of the Royal Meteorological Society*, 137, 176–189. <https://doi.org/10.1002/qj.760>
- Berner, J., Ha, S.-Y., Hacker, J. P., Fournier, A., & Snyder, C. (2011). Model uncertainty in a mesoscale ensemble prediction system: Stochastic vs. multiphysics representations. *Monthly Weather Review*, 139, 1972–1995. <https://doi.org/10.1175/2010MWR3595.1>
- Byers, H. R., & Rodebush, H. R. (1948). Causes of thunderstorms of the Florida Peninsula. *Journal of Meteorology*, 5, 275–280. [https://doi.org/10.1175/1520-0469\(1948\)005<0275:COTOTF>2.0.CO;2](https://doi.org/10.1175/1520-0469(1948)005<0275:COTOTF>2.0.CO;2)
- Caracena, F., Maddox, R. A., Hoxit, L. R., & Chappell, C. F. (1979). Mesoanalysis of the Big Thompson storm. *Monthly Weather Review*, 107, 1–17. [https://doi.org/10.1175/1520-0493\(1979\)107<0001:MOTBTS>2.0.CO;2](https://doi.org/10.1175/1520-0493(1979)107<0001:MOTBTS>2.0.CO;2)
- Cohuet, J. B., Romero, R., Homar, V., Ducrocq, V., & Ramis, C. (2011). Initiation of a severe thunderstorm over the Mediterranean Sea. *Atmospheric Research*, 100, 603–620. <https://doi.org/10.1016/j.atmosres.2010.11.002>
- Corsmeier, U., Kalthoff, N., Barthlott, C., Aoshima, F., Behrendt, A., Di Girolamo, P., et al. (2011). Processes driving deep convection over complex terrain: A multiscale analysis of observations from COPS IOP 9c. *Quarterly Journal of the Royal Meteorological Society*, 137, 137–155. <https://doi.org/10.1002/qj.754>
- Dai, Y., Williams, I. N., & Qiu, S. (2021). Simulating the effects of surface energy partitioning on convective organization: Case study and observations in the US Southern Great Plains. *Journal of Geophysical Research: Atmospheres*, 126, e2020JD033821. <https://doi.org/10.1029/2020JD033821>
- Du, Y., Chen, G., Han, B., Bai, L., & Li, M. (2020). Convection initiation and growth at the coast of South China. Part II: Effects of the terrain, coastline, and cold pools. *Monthly Weather Review*, 148, 3871–3892. <https://doi.org/10.1175/MWR-D-20-0090.1>
- Du, Y., Chen, G., Han, B., Mai, C., Bai, L., & Li, M. (2020). Convection initiation and growth at the coast of South China. Part I: Effect of the marine boundary layer jet. *Monthly Weather Review*, 147, 3847–3869. <https://doi.org/10.1175/MWR-D-20-0089.1>
- Duffourg, F., Nuissier, O., Ducrocq, V., Flamant, C., Chazette, P., Delanoë, J., et al. (2015). Offshore deep convection initiation and maintenance during the HyMeX IOP 16a heavy precipitation event. *Quarterly Journal of the Royal Meteorological Society*, 142, 259–274. <https://doi.org/10.1002/qj.2725>
- Grant, L. D., Lane, T. P., & van den Heever, S. C. (2018). The role of cold pools in tropical oceanic convective systems. *Journal of the Atmospheric Sciences*, 75, 2615–2634. <https://doi.org/10.1175/JAS-D-17-0352.1>
- Grell, G. A., & Freitas, S. R. (2014). A scale and aerosol aware stochastic convective parameterization for weather and air quality modeling. *Atmospheric Chemistry and Physics*, 14, 5233–5250. <https://doi.org/10.5194/acp-14-5233-2014>
- Hamill, T. M., & Colucci, S. J. (1997). Verification of Eta-RSM short-range ensemble forecasts. *Monthly Weather Review*, 125, 1312–1327. [https://doi.org/10.1175/1520-0493\(1997\)125<1312:VOERSR>2.0.CO;2](https://doi.org/10.1175/1520-0493(1997)125<1312:VOERSR>2.0.CO;2)
- Hitchens, N. M., Brooks, H. E., & Schumacher, R. S. (2013). Spatial and temporal characteristics of heavy hourly rainfall in the United States. *Monthly Weather Review*, 141, 4564–4575. <https://doi.org/10.1175/MWR-D-12-00297.1>
- Hong, S. Y., Noh, Y., & Dudhia, J. (2006). A new vertical diffusion package with an explicit treatment of entrainment processes. *Monthly Weather Review*, 134, 2318–2341. <https://doi.org/10.1175/MWR3199.1>
- Houze, R. A., Jr. (2012). Orographic effects on precipitating clouds. *Review of Geophysics*, 50, RG1001. <https://doi.org/10.1029/2011RG000365>
- Houze, R. A., Jr., Wilton, D. C., & Smull, B. F. (2007). Monsoon convection in the Himalaya region as seen by the TRMM Precipitation Radar. *Quarterly Journal of the Royal Meteorological Society*, 133, 1389–1411. <https://doi.org/10.1002/qj.106>
- Huang, Y., Liu, Y., Liu, Y., & Knievel, J. (2019). Budget analyses of a record-breaking rainfall event in the coastal metropolitan city of Guangzhou, China. *Journal of Geophysical Research: Atmospheres*, 124, 9391–9406. <https://doi.org/10.1029/2018JD030229>
- Huang, Y., Liu, Y., Liu, Y., Li, H., & Knievel, J. (2019). Mechanisms for a record-breaking rainfall in the coastal metropolitan city of Guangzhou, China: Observation analysis and nested very-large-eddy simulation with the WRF Model. *Journal of Geophysical Research: Atmospheres*, 124, 1370–1391. <https://doi.org/10.1029/2018JD029668>
- Huang, Y., Wang, Y., Xue, L., Wei, X., Zhang, L., & Li, H. (2020). Comparison of three microphysics parameterization schemes in the WRF model for an extreme rainfall event in the coastal metropolitan City of Guangzhou, China. *Atmospheric Research*, 240, 104939. <https://doi.org/10.1016/j.atmosres.2020.104939>

- Iacono, M. J., Delamere, J. S., Mlawer, E. J., Shephard, M. W., Clough, S. A., & Collins, W. D. (2008). Radiative forcing by long-lived greenhouse gases: Calculations with the AER radiative transfer models. *Journal of Geophysical Research*, 113, D13103. <https://doi.org/10.1029/2008JD009944>
- James, R. P., Fritsch, J. M., & Markowski, P. M. (2005). Environmental distinctions between cellular and slabular convective lines. *Monthly Weather Review*, 133, 2669–2691. <https://doi.org/10.1175/MWR3002.1>
- Khairoutdinov, M., & Randall, D. (2006). High-resolution simulation of shallow-to-deep convection transition over land. *Journal of the Atmospheric Sciences*, 63, 3421–3436. <https://doi.org/10.1175/JAS3810.1>
- Kingsmill, D. E. (1995). Convection initiation associated with a sea-breeze front, a gust front, and their collision. *Monthly Weather Review*, 123, 2913–2933. [https://doi.org/10.1175/1520-0493\(1995\)123<2913:CIAWS>2.0.CO;2](https://doi.org/10.1175/1520-0493(1995)123<2913:CIAWS>2.0.CO;2)
- Lean, H. W., Roberts, N. M., Clark, P. A., & Morcrette, C. (2009). The surprising role of orography in the initiation of an isolated thunderstorm in southern England. *Monthly Weather Review*, 137, 3026–3046. <https://doi.org/10.1175/2009MWR2743.1>
- Lee, J. T., Lee, D. I., Shimizu, S., & You, C. H. (2019). Analysis of determinants for an enhanced and long-lasting coastal convective system by means of a case study (July 26, 2011). *Advances in Atmospheric Sciences*, 36, 1327–1339. <https://doi.org/10.1007/s00376-019-9025-x>
- Li, H., Cui, X., & Zhang, D. L. (2017a). On the initiation of an isolated heavy-rain-producing storm near the central urban area of Beijing Metropolitan Region. *Monthly Weather Review*, 145, 181–197. <https://doi.org/10.1175/MWR-D-16-0115.1>
- Li, H., Cui, X., & Zhang, D. L. (2017b). Sensitivity of the initiation of an isolated thunderstorm over the Beijing Metropolitan Region to urbanization, terrain morphology and cold outflows. *Quarterly Journal of the Royal Meteorological Society*, 143, 3153–3164. <https://doi.org/10.1002/qj.3169>
- Li, Z., Luo, Y., Du, Y., & Chan, J. C. L. (2020). Statistical characteristics of pre-summer rainfall over South China and associated synoptic conditions. *Journal of the Meteorological Society of Japan*, 98, 213–233. <https://doi.org/10.2151/jmsj.2020-012>
- Liang, Z., Wang, D., Liu, Y., & Cai, Q. (2017). A numerical study of the convection triggering and propagation associated with sea breeze circulation over Hainan Island. *Journal of Geophysical Research: Atmosphere*, 122, 8567–8592. <https://doi.org/10.1002/2016JD025915>
- Lima, M. A., & Wilson, J. W. (2008). Convective storm initiation in a moist tropical environment. *Monthly Weather Review*, 136, 1847–1864. <https://doi.org/10.1175/2007MWR2279.1>
- Lin, Y. L., Chiao, S., Wang, T. A., Kaplan, M. L., & Weglarz, R. P. (2001). Some common ingredients for heavy orographic rainfall. *Weather and Forecasting*, 16, 633–660. [https://doi.org/10.1175/1520-0434\(2001\)016<0633:SCIFHO>2.0.CO;2](https://doi.org/10.1175/1520-0434(2001)016<0633:SCIFHO>2.0.CO;2)
- Liu, Y., Zhuang, X., & Li, X. (2001). Severe local storms initiated by the sea breeze front in the Pearl River Delta during the late spring and summer. *Journal of Applied Meteorological Science*, 12, 433–441.
- Lombardo, K., & Colle, B. A. (2010). The spatial and temporal distribution of organized convective structures over the Northeast and their ambient conditions. *Monthly Weather Review*, 138, 4456–4474. <https://doi.org/10.1175/2010MWR3463.1>
- Luo, Y., Wu, M., Ren, F., Li, J., & Wong, W.-K. (2016). Synoptic situations of extreme hourly precipitation over China. *Journal of Climate*, 29, 8703–8719. <https://doi.org/10.1175/jcli-d-16-0057.1>
- Luo, Y., Zhang, R., Wan, Q., Wang, B., Wong, W. K., Hu, Z., et al. (2017). The Southern China Monsoon Rainfall Experiment (SCMREX). *Bulletin of the American Meteorological Society*, 98, 999–1013. <https://doi.org/10.1175/JCLI-D-16-0057.1>
- Mansell, E. R., Ziegler, C. L., & Bruning, E. C. (2010). Simulated electrification of a small thunderstorm with two-moment bulk microphysics. *Journal of the Atmospheric Sciences*, 67, 171–194. <https://doi.org/10.1175/2009JAS2965.1>
- Marwitz, J. D. (1983). The kinematics of orographic airflow during Sierra storms. *Journal of the Atmospheric Sciences*, 40, 1218–1227. [https://doi.org/10.1175/1520-0469\(1983\)040<1218:TKOOAD>2.0.CO;2](https://doi.org/10.1175/1520-0469(1983)040<1218:TKOOAD>2.0.CO;2)
- Mattos, E. V., & Machado, L. A. T. (2011). Cloud-to-ground lightning and mesoscale convective systems. *Atmospheric Research*, 99, 377–390. <https://doi.org/10.1016/j.atmosres.2010.11.007>
- Meng, W., Zheng, Y., Wang, B., Zhang, Y., Jiang, D., Yuan, J., & Luo, C. (2014). Observational and numerical study of impacts of interactions between heat island and sea-breeze on the late-afternoon severe precipitation over Pearl River Delta. *Journal of Tropical Meteorology*, 30, 1011–1026. <https://doi.org/10.3969/j.issn.1004-4965.2014.06.002>
- Miao, J. E., & Yang, M. J. (2020). A modeling study of the severe afternoon thunderstorm event at Taipei on June 14, 2015: The roles of sea breeze, microphysics, and terrain. *Journal of the Meteorological Society of Japan*, 98, 129–152. <https://doi.org/10.2151/jmsj.2020-008>
- Purdom, J. F. W. (1976). Some uses of high resolution GOES imagery in the mesoscale forecasting of convection and its behavior. *Monthly Weather Review*, 104, 1474–1483. [https://doi.org/10.1175/1520-0493\(1976\)104<1474:SUOHRG>2.0.CO;2](https://doi.org/10.1175/1520-0493(1976)104<1474:SUOHRG>2.0.CO;2)
- Rasmussen, K. L., & Houze, R. A., Jr. (2016). Convective initiation near the Andes in subtropical South America. *Monthly Weather Review*, 144, 2351–2374. <https://doi.org/10.1175/2015MWR-D-15-0058.1>
- Rodrigues, M. L. G., & Ynoue, R. Y. (2016). Mesoscale and synoptic environment in three orographically enhanced rain events on the coast of Santa Catarina (Brazil). *Weather and Forecasting*, 31, 1529–1546. <https://doi.org/10.1175/WAF-D-15-0003.1>
- Romatschke, U., & Houze, R. A., Jr. (2011). Characteristics of precipitating convective systems in the south Asian monsoon. *Journal of Hydrometeorology*, 12, 3–26. <https://doi.org/10.1175/2010JHM1289.1>
- Romatschke, U., Medina, S., & Houze, R. A., Jr. (2010). Regional, seasonal, and diurnal variations of extreme convection in the South Asian region. *Journal of Climate*, 23, 419–439. <https://doi.org/10.1175/JCLI3140.1>
- Rotunno, R., Klemp, J. B., & Weisman, M. L. (1988). A theory for strong, long-lived squall lines. *Journal of the Atmospheric Sciences*, 45, 463–485. [https://doi.org/10.1175/1520-0469\(1988\)045<0463:ATFSLL>2.0.CO;2](https://doi.org/10.1175/1520-0469(1988)045<0463:ATFSLL>2.0.CO;2)
- Schneidereit, M., & Schär, C. (2000). Idealised numerical experiments of Alpine flow regimes and southside precipitation events. *Meteorology and Atmospheric Physics*, 72, 233–250. <https://doi.org/10.1007/s007030050018>
- Schwartz, C. S., Kain, J. S., Weiss, S. J., Xue, M., Bright, D. R., Kong, F., et al. (2010). Toward improved convection-allowing ensembles: Model physics sensitivities and optimizing probabilistic guidance with small ensemble membership. *Weather and Forecasting*, 25, 263–280. <https://doi.org/10.1175/2009WAF2222267.1>
- Skamarock, W. C., Klemp, J. B., Dudhia, J., Grill, D. O., Barker, D., Duda, M. G., et al. (2008). *A description of the advanced research WRF version 3 (No. NCAR/TN-475+STR)*. University Corporation for Atmospheric Research. <https://doi.org/10.5065/D68S4MVH>
- Tu, C. C., Chen, Y. L., Chen, C. S., Lin, P. L., & Lin, P. H. (2014). A comparison of two heavy rainfall events during the Terrain-Induced Monsoon Rainfall Experiment (TiMREX) 2008. *Monthly Weather Review*, 142, 2436–2463. <https://doi.org/10.1175/MWR-D-13-00293.1>
- Wang, C. C., Chen, G. T. J., Chen, T. C., & Tsuboki, K. (2005). A numerical study on the effects of Taiwan topography on a convective line during the Mei-Yu season. *Monthly Weather Review*, 133, 3217–3242. <https://doi.org/10.1175/MWR3028.1>
- Wang, C. C., & Kirshbaum, D. J. (2015). Thermally forced convection over a mountainous tropical island. *Journal of the Atmospheric Sciences*, 72, 2482–2506. <https://doi.org/10.1175/JAS-D-14-0325.1>
- Wang, H., Luo, Y., & Jou, B. J. D. (2014). Initiation, maintenance and properties of convection in an extreme rainfall event during SCMRES: Observational analysis. *Journal of Geophysical Research: Atmosphere*, 119, 206–232. <https://doi.org/10.1002/2014JD022339>

- Wapler, K., & Lane, T. (2012). A case of offshore convective initiation by interacting land breezes near Darwin, Australia. *Meteorology and Atmospheric Physics*, 115, 123–137. <https://doi.org/10.1007/s00703-011-0180-6>
- Weckwerth, T. M., Bennett, L. J., Miller, L. J., Van Baelen, J., Di Girolamo, P., Blyth, A. M., & Hertnecky, T. J. (2014). An observational and modeling study of the processes leading to deep, moist convection in complex terrain. *Monthly Weather Review*, 142, 2687–2708. <https://doi.org/10.1175/MWR-D-13-00216.1>
- Weckwerth, T. M., & Wakimoto, R. M. (1992). The initiation and organization of convective cells atop a cold-air outflow boundary. *Monthly Weather Review*, 120, 2169–2187. [https://doi.org/10.1175/1520-0493\(1992\)120<2169:TIAOOC>2.0.CO;2](https://doi.org/10.1175/1520-0493(1992)120<2169:TIAOOC>2.0.CO;2)
- Weisman, M. L., & Rotunno, R. (2004). “A theory for strong long-lived squall lines” revisited. *Journal of the Atmospheric Sciences*, 61, 361–382. [https://doi.org/10.1175/1520-0469\(2004\)061<0361:ATFSLS>2.0.CO;2](https://doi.org/10.1175/1520-0469(2004)061<0361:ATFSLS>2.0.CO;2)
- Whiteman, C. D. (2000). *Mountain meteorology*. Oxford University Press.
- Wilhelmsen, R. B., & Chen, C. S. (1982). A simulation of the development of successive cells along a cold outflow boundary. *Journal of the Atmospheric Sciences*, 39, 1466–1483. [https://doi.org/10.1175/1520-0469\(1982\)039<1466:ASOTDO>2.0.CO;2](https://doi.org/10.1175/1520-0469(1982)039<1466:ASOTDO>2.0.CO;2)
- Wilson, J. W., & Mueller, C. K. (1993). Nowcasts of thunderstorm initiation and evolution. *Weather and Forecasting*, 8, 113–131. [https://doi.org/10.1175/1520-0434\(1993\)008<0113:NOTIAE>2.0.CO;2](https://doi.org/10.1175/1520-0434(1993)008<0113:NOTIAE>2.0.CO;2)
- Wu, F., & Lombardo, K. (2021). Precipitation enhancement in squall lines moving over mountainous coastal regions. *Journal of the Atmospheric Sciences*, 78, 3089–3113. <https://doi.org/10.1175/JAS-D-20-0222.1>
- Wu, M., & Luo, Y. (2016). Mesoscale observational analysis of lifting mechanism of a warm-sector convective system producing the maximal daily precipitation in China mainland during pre-summer rainy season of 2015. *Journal of Meteorological Research*, 30, 719–736. <https://doi.org/10.1007/s13351-016-6089-8>
- Wu, N., Ding, X., Wen, Z., Chen, G., Meng, Z., Lin, L., & Min, J. (2020). Contrasting frontal and warm-sector heavy rainfalls over South China during the early-summer rainy season. *Atmospheric Research*, 235, 104693. <https://doi.org/10.1016/j.atmosres.2019.104693>
- Xu, W., Zipser, E. J., Chen, Y. L., Liu, C., Liou, Y. C., Lee, W. C., & Jou, B. J. D. (2012). An orography-associated extreme rainfall event during TiMREX: Initiation, storm evolution, and maintenance. *Monthly Weather Review*, 140, 2555–2574. <https://doi.org/10.1175/MWR-D-11-00208.1>
- Zhong, S. X., & Tian, F. Y. (2020). The heavy rainfall during the warm season over the Pearl River Delta region: Movements and early signals. *Atmospheric Science Letters*, 22, e1012. <https://doi.org/10.1002/asl.1012>
- Zhuang, X., Xue, M., Wu, N., Min, J., & Kong, F. (2021). Error growth dynamics within convection-allowing ensemble forecasts over central U.S. regions for days of active convection. *Monthly Weather Review*, 149, 959–977. <https://doi.org/10.1175/MWR-D-20-0329.1>